FORTIFIKATORISK

NOTAT NR. 82 / 72

UNDERGROUND AMMUNITION STORAGE

Blast propagation in the tunnel system

Report IV A

Connected Chamber Storage. Variable Chamber Volume and Variable Angle between Branch and Main Passageway

FORSVARETS BYGNINGSTJENESTE

NORWEGIAN DEFENCE CONSTRUCTION SERVICE
Office of Test and Development

(14) Fortifikatorisk notat ~~nr~~ 82/72

(6) UNDERGROUND AMMUNITION STORAGE.

Blast propagation in the tunnel system.

Report IV A.

Connected Chamber Storage. Variable Chamber Volume and Variable Angle between Branch and Main Passageway.

(10) A.T. Skjeltorp, T. Hegdahl ~~and~~ A. Jonssen

(11) Nov 75

(12) 48 p.

November 1975

NORWEGIAN DEFENCE CONSTRUCTION SERVICE
Office of Test and Development

Fortifikatorisk notat nr 82/72

UNDERGROUND AMMUNITION STORAGE

Blast propagation in the tunnel system

Report IV A

Connected Chamber Storage. Variable Chamber Volume and Variable Angle between Branch and Main Passageway

A.T. Skjeltorp, T. Hegdahl, and A. Jenssen

November 1975

TABLE OF CONTENTS

ABSTRACT

Model tests have been performed to determine the blast wave propagation in the tunnel system of underground ammunition storage sites with connected storage chambers. A total of 18 different configurations were tested with variable chamber volumes (300 - 15200 cc), angles between the branch- and main passage-way (35° - 90°), and ratios between the cross sections of the branch- and main passage-way (0,125 - 0,5). The models were in linear scales 1:40 to 1:100 of typical full scale installations. By analysing the data, it was possible to obtain relatively simple scaling relationships which contain all of the most important geometrical parameters.

The model data are compared with one large scale test and fair agreement is found.

1. INTRODUCTION

This report is the fourth in a series of five /1 - 5/ describing the results from an extensive series of model tests on underground ammunition storage in case of accidental explosions. In two preceeding reports /2, 3/, measurements were presented on the pressures in the storage chamber and the air blast in the tunnel system of a single chamber storage site, respectively. The present report deals with the problem of blast wave propagation in the tunnel systems of connected chamber storage sites.

The prevention of propagation of an explosion from one chamber to another is of major concern in the planning of connected chamber storage sites, and protective blast doors, blast walls, etc. of sufficient strength are required.

The results from the present model tests will provide the designer blast data for engineering use for a wide range of typical storage site configurations.

The present results will also serve as a starting point in the determination of external safety distances as these in principle can be determined from the blast at the exit of the main passageway. This problem will be discussed in a later report.

The basic scaling laws used in the present work will be discussed in Sec. 2, followed by a short presentation of the experimental details in Sec. 3. The experimental results will be presented and discussed in Sec. 4, and the principal results are finally summarized in Sec. 5.

2. THEORETICAL CONSIDERATIONS

2.1 Scaling Relationships

The basis for the scaling relationships proposed in the present report is the familiar Hopkinson's scaling laws /6/, which were reviewed in Report I /1/. In the analysis of the results for single chamber storage sites in Report III A /3/, various geometrical parameters were incorporated in a nondimensional form and provided quite general scaling relationships. This technique will also be attempted for the present experiments.

Fig. 2.1 shows a cross-section of a typical connected chamber storage site including also the definitions of the parameters believed to be of primary importance. Simple similtude analysis coupled with empirical observations of the present test results, have produced the following scaling relationships for peak pressure p, impulse I, and positive duration t_+:

$$p = f(QX_{\pm}/V_t,\ A_j'/A_k) \tag{2.1a}$$

$$IA_k/Q = g(QX_{\pm}/V_t,\ A_j'/A_k) \tag{2.1b}$$

$$t_+A_k/Q = h\ (QX_{\pm}/V_t,\ A_j'/A_k) \tag{2.1c}$$

Referring to Fig. 2.1,

$$V_t = V_i + A_j'L' + A_k2L, \tag{2.1d}$$

or combined volume of the storage chamber, V_i, the branch passage-way, $A_j'L'$, and twice the volume of the main passage-way out to the observation point, A_k2L. Furthermore, $X_{\pm}$ expresses the energy distribution in the two directions of the main passage-way.

Earlier tests /7/ have indicated that

$$X_+ = 2(1 - v_m/180^o)$$

$$X_- = v_m/90^o \qquad (2.1e)$$

X_+ is simply a short form to express that either X_+^- or X_- is to be used for the evaluation of the blast wave parameters in the positive or the negative direction of the tunnel, respectively (see def. in Fig. 2.1). It can be seen that the definitions in Eq. (2.1e) satisfy the boundary conditions in that

$$X_+ = X_- \text{ for } v_m = 90^o,$$

i.e. symmetric energy distribution, and for $v_m = 180^o$:

$$X_+ = 0$$

$$X_- = 1$$

Likewise, for $v_m = 0^o$

$$X_+ = 1$$

$$X_- = 0$$

For these two particular cases, Eqs. (2.1a) - (2.1c) reduce to the scaling relationships employed in Report III A for single chamber storage sites.

Thus, QX_+/V_t in the proposed scaling relationships represents an effective loading density including not only the chamber volume and tunnel volumes, but also the energy distribution for variable angles v_m.

Obviously, the cross-sectional areas of the branch- and main passage-way wil also effect the blast propagation and this is represented by the ratio, A_j'/A_c.

The functional form of the proposed scaling relationships has to be established by the experimental results, which will be discussed in Sec. 4.

2.2 Non-Scaling Energy Losses

The simple scaling laws proposed in Sec. 2.1 do no account for energy dissipating effects such as thermal energy transmission to the walls, elastic or inelastic deformation of the walls, and viscous loss due to wall roughness. Of these effects, only the loss due to wall roughness is espected to influence significantly the blast propagation, but then only over long distances and/or on the case of large roughness. This is discussed in Report I.

According to a model originally proposed by Porzel /8/, the peak pressure attenuation may be expressed as:

$$Y(p) = \text{constant} - 2\epsilon(\bar{e}/D)(L/D) \qquad (2.2a)$$

Here, Y(p) is an impedance function defined as

$$Y(p) = \frac{13}{7}\ln p - \frac{6}{7}\ln(p + 7) - \frac{1}{p} \qquad (2.2b)$$

with p the pressure at a distance L/D along the tunnel. The ratio $\bar{e}/D$ is the average relative wall roughness and ϵ an efficiency factor in the range $1/2 \leq \epsilon \leq 1$.

For the relatively smooth-walled steel tubes used in the present tests, the effects of the wall roughness is expected to be relatively small, and will be discussed in more detail in Sec. 4.

3. EXPERIMENTAL DETAILS

Details of the models, instrumentation, and data reduction are to be found in Report I /1/, and we shall therefore only summarize the main feature here.

The test programme was designed to determine the blast wave propagation in the main passageway of typical connected chamber storage sites. A total of nine combinations of chamber volumes and tunnel cross sections were used as shown in Fig. 3.a. Most loading densities varied between 3 and 70 kg/m^3 and pressure-time history was recorded in most cases at six different distances from the storage chamber, ranging from approximately 2 to 80 tunnel diameters.

The TNT charges used in the tests were suspended in the middle of the detonation chamber and initiated with electrical blasting cap no. 8. This has an equivalent TNT weight of 1,5 $\pm$ 0,5 g. The smallest charges used in the tests were 8 g TNT and the uncertainty in the loading density stemming from the blasting cap is therefore less than 6%.

To measure the pressure-time history in the models, standard measurement techniques were used and the blast wave parameters were evaluated using special computer programmes. The total uncertainty in the peak pressure was estimated to be about 10%, whereas the uncertainty in the impulse was estimated to be about 30%.

4. EXPERIMENTAL RESULTS AND ANALYSIS

A total of approximately 1500 blast wave parameter values (peak pressure, impulse and positive duration) were obtained for the 18 configurations discussed in Sec. 3. The results from tests reported earlier on connected chamber storage sites /7/ have also been included in the present report. These earlier data combined with the present results thus provided the 18 configurations in Fig. 3.a. Only the most significant results will be presented here since part B of this report contains all the pressure-time recordings and tabulated blast wave parameters except for pressure-time recordings from the earlier tests /7/.

The purpose of the analysis that follows are (1) to determine qualitatively and quantitatively the dependence of peak pressure, impulse and positive duration according to the scaling relationship proposed in Sec. 2, and (2) to establish empirical relationships that identify the more important factors taht can be applied to blast predictions for underground storage sites geometrically similar to the present range of models. It should be emphasized that the final analysis are empirical and statistical in approach.

4.1 Peak Pressure Scaling Relationships

The basic quantity of interest in the present model tests is the peak side-on overpressure p in the passageway. In Fig. 4.1a, p is plotted versus L/D with the loading density Q/V_i as parameter for one typical configuration. Fig. 4.1b shows the same data plotted versus Q/V_i with L/D as parameter. These plots are in socalled dimensionless form, i.e. independent the linear scaling factor n. (See Report I /1/).

Letting subscripts F and N denote full scale and model respectively,

$$p_F = p_M, \tag{4.1a}$$

and $L_F/D_F = nL_M/nD_M = L_M/D_M$.

For the loading density,

$$Q_F/V_F = n^3Q_M/n^3V_M = Q_M/V_M \tag{4.1b}$$

The results in Figs. 4.1a and 4.1b may therefore in principle be used for any geometrically similar systems. However, it is of interest to reduce the number of curves necessary to characterize the blast wave propagation in this particular system. In Sec. 2.1, it was proposed to scale the data

according to $QX_{\pm}/V_t$, where now V_t is the total volume of the chamber and the tunnel out to the observation point. Fig. 4.1c shows the results in this presentation for the same data as before, notably with $X_{\pm} = 1$ according to the definition in Eq. (2.1e). As may be seen, the data points are evenly distributed around one straight line. This means that one universal curve appears to reproduce the tunnel pressure at any point in the tunnel for any charge Q for the present range of measurements.

Figs. 4.1d - 4.1i show the variation of p versus $QX_{\pm}/V_t$ for all the 18 configurations in the tests with v_m, A_j'/A_k, and V_i as parameters. In Fig. 4.1j, the peak pressure data are compared for four widely different chamber volumes.

From Figs 4.1d - 4.1f it may be seen that there is a systematic decrease in pressure for decreasing values of A_j'/A_k. The results in Figs. 4.1g - 4.1i show that p is on the average a unique function of $QX_{\pm}/V_t$ for different values of the angle v_m.
In Fig. 4.1j, the peak pressure data are compared for four widely different chamber volumes V_i with $A_j'/A_k = 1/2$ and $v_m = 90^o$. As may be seen, the data are relatively insensitive to the value of V_i.

The qualitative observations made here will be tested more systematically in the following sections which contains the results from various empirical fits.

4.1.1 Comparisons of Geometrically Similar Models

Of the 18 different models listed in Fig. 3.a, only two were exactly geometrically similar:

Model 1 $V_i = 800\ cm^3$

$A_j' = 10\ cm^2$

$A_k = 20\ cm^2$

$v_m = 90^o$

Model 2 $V_i = 15200\ cm^3$

$A_j' = 70\ cm^2$

$A_k = 140\ cm^2$

$v_m = 90^o$

The linear scaling factor between Model 1 and 2 is n = 2,6 and in linear scales 1:100 and 1:38 of typical full scale sites with $A_k = 20\ m^2$.

Figs. 4.1.1a and 4.1.1b compares the peak pressure data at two scaled distances L/D = 11 and L/D = 20, respectively. There is good agreement between the two sets of data in Fig. 4.1.1a, but in Fig.4.1.1b the pressures for Model 1 appear to be consistently lower than those for Model 2. This difference is in fact consistent with the effects of wall roughness attenuation according to the model discussed in Sec. 2.2. Letting p_o denote the fictitious "smooth-walled" pressures and p_1 and p_2 the recorded pressures for Model 1 and Model 2 respectively, Eq. (2.2a) can be expressed as:

$$Y(p_o) - Y(p_1) = 2\epsilon\bar{e}/D_1(L/D) \qquad (4.1.1a)$$

for Model 1 (D_1 = 50 mm), and

$$Y(p_o) - Y(p_2) = 2\epsilon\bar{e}/D_2(L/D) \qquad (4.1.1b)$$

for Model 2 (D_2 = 134,5 mm).

The effective average wall roughness $2\epsilon\bar{e}$ in units of mm is assumed to be the same in both models.

Thus, from Eqs (4.1.1a) and (4.1.1b),

$$Y(p_2) - Y(p_1) = 2\epsilon\bar{e}(1/D_1 - 1/D_2)\ (L/D) \qquad (4.1.1c)$$

This coupled with the results in Fig. 4.1.1b produces

$$2\epsilon\bar{e} \simeq 0{,}8 \pm 0{,}5 \text{ mm}$$

As $\epsilon \simeq 1$ for small L/D-values /1/, $\bar{e} \simeq 0{,}4 \pm 0{,}3$ mm, which is consistent with the direct measured wall roughness.

These limited sets of data thus rule out the presence of significant non-scaling energy losses discussed in Sec. 2.2. (conduction, radiation, elastic or inelastic deformation of the walls).

4.1.2 Test of Energy Distribution

It was postulated in Sec. 2.1, Eq. (2.1a), that the peak pressure will be a unique function of the effective loading density, $QX_{\pm}/V_t$, which contains the energy distribution factor $\bar{X}_{\pm}$ defined in Eq. (2.1e).

As an example, Fig. 4.1.2a shows the data for one particular case with $v_m = 35^o$ to check the adequateness of this proposed energy division. Under the assumption of a linear functional dependence in a log-log plot

$$p = C_1(QX_{\pm}/V_t)^{C_2}, \qquad (4.1.2a)$$

least squares fits of the two sets of data produced the parameters:

$$\left.\begin{aligned} C_1 &= 7{,}1 \pm 1{,}1 \\ C_2 &= 0{;}52 \pm 0{,}05 \end{aligned}\right\} \text{ for } X+$$

$$\left.\begin{aligned} C_1 &= 6{,}2 \pm 1{,}1 \\ C_2 &= 0{,}53 \pm 0{,}02 \end{aligned}\right\} \text{ for } X-$$

Clearly, for these particular sets of data, the proposal energy distribution is adequate. Similar checks for the remaining 5 configurations in Fig. 3.a with $v_m = 90^o$ provided similar results.

4.1.3 Empirical Scaling Relationships

This section lists three methods examined for scaling the peak pressure data.

Method a

From the empirical observations exemplified in the preceeding sections, it is postulated that the peak pressure may be expressed as (A_j'/A_k = constant):

$$p = B_1(QX_{\pm}/V_t)^{B_2} \qquad (4.1.3a)$$

where:

B_1 = scaling factor

B_2 = scaling exponent

Least squares fits of Eq (4.1.3a) were made to the data for each of the 18 configurations in Fig. 3.a. Figs. 4.1d - 4.1i display all the data together with curves resulting from this fitting procedure. The corresponding scaling parameters B_1 and B_2 are given in Table 4.1.3a, from which it can be seen that there appears to be no systematic variations in B_1 and B_2 for different chamber volumes for the same value of A_j'/A_k. An exception is the results for the V_i = 300 cm3 chamber volume, which produced significantly higher B_1-values and lower B_2-values than those for the other configurations. It may also be noted from Table 4.1.3a that for decreasing values of A_j'/A_k, there is on the average a distinct systematic decrease in the value for B_1, whereas B_2 appears to show little variation.

On the whole, the empirical fits reproduce the data remarkably well as seen from the error column in Table 4.1.3a. The average error for all measurements is approximately 14%. This is quite satisfactory considering the estimated 10% experimental uncertainty in the peak pressure determination.

Method b

The second method used to scale the peak pressures included the effects from the variation of A_j'/A_k:

$$p = C_1(QX_{\pm}/V_t)^{C_2}\,(A_j'/A_k)^{C_3} \qquad (4.1.3b)$$

This equation was fitted to all 18 configurations with C_1, C_2, and C_3 as adjustable parameters. The results of this procedure are shown in Table 4.1.3b.

Method c

The third method used to scale the peak pressures included also the effects from the variation of A_j'/A_k and possible effects from wall roughness attenuation:

$$p_o = D_1(Qx_{\pm}/V_t)^{D_2} (A_j'/A_k)^{D_3} \qquad (4.1.3c)$$

$$Y(p_o) - Y(p) = (D_4/D)(L/D) \qquad (4.1.3d)$$

where:

p_o = fictitious peak pressure without wall friction

p = measured peak pressure

$Y(p_o)$ = impedance function of p_o, Eq.(2.2b)

$Y(p)$ = impedance function of p, Eq. (2.2b)

D_1, D_2, D_3 = scaling parameters

$D_4 = 2 \epsilon \bar{e}$ = effective wall roughness, see Report I.

The data for all 18 configurations were fitted to Eqs. (4.1.3c) and (4.1.3d). The results of this procedure are shown in Table 4.1.3c. As may be seen, the value for D_4 is rather small, but negative, which is not consistent with the proposed model. However, within the stated error limits, D_4 may in fact be zero, and the fit therefore shows that the average wall roughness must be small in accordance with the use of the relatively smooth-walled steel tubes in tests.

4.1.4 Evaluation of the Empirical Fits

On the basis of the results from the three different

empirical fits found in the preceeding section, there are three major conclusions which may be reached:

i) Induvidual fits to each of the 18 configurations (Method a) reproduce the data within approximately the expected experimental scatter (10%).

ii) Method b) excluding the effects from wall roughness and method c) including these effects do not produce significantly different scaling parameters. This shows that the tube wall roughness is small.

iii) Method a) reproduces the data better (14%) than method b) (20%). However, the convenience of being able to represent all the data in one formula favours the use of method b).

As a general conclusion it is therefore recommended to use the results from method b) in Table 4.1.3b in the prediction of the smooth wall peak pressure, i.e.:

$$p = (10,0 \pm 0,6)(QX_{\pm}/V_t)^{0,55\pm0,02}(A_j'/A_c)^{0,61\pm0,06} \qquad (4.1.4)$$

Here, a 2σ standard deviation (96% confidence interval) has been used on the scaling parameters.

There are various limitations imposed on the present results for which the simple relationship in Eq.(4.1.4) is expected to be invalid. This has been discussed in Report III. In particular, for significat tunnel wall roughness, Eq.(4.1.4) may be supplemented by the use of the impedance function as outlined earlier in this section and in Report I /1/. As has been discussed elsewhere /9/, the wall roughness attenuation may be considerable for typical tunnels blasted out of rock, and the use of Eq. (4.1.4) will be quite conservative or on the safe side.

4.2 Scaling Relationships for Impulse

The results for the impulse are much more difficult to combine empirically in a straightforward way than

those for the front pressure. This is partly due to the significantly larger uncertainties involved here and special features are not easily discernible. This is clear from the typical results in Fig. 4.2a. On the average, the impulse decreases slowly with distance from the storage chamber, but there is no systematically large drop near the chamber as was observed for front pressure.

To test the proposed scaling hypothesis in Sec. 2.1, Eq. (2.1b), the results in Fig. 4.2a are shown in Fig. 4.2b as $I\,A_k/Q$ versus Q/V_t. To a first approximation the results fall on discrete curves with L/D as a parameter. Part, or all of the L/D-dependence may be due to the wall roughness, but so far it has not been possible to account for this theoretically.

Figs. 4.2c and 4.2d show the scaled impulse data for the two geometrically similar models, Model 1 and Model 2, which were discussed earlier in Sec. 4.1.1. As may be seen, there is good agreement between the two sets of data.

Fig. 4.2e shows a test of the proposed energy distribution represented by X_+. As may be seen, at the same scaled distance L/D, the scaled impulse data appear to be adequately reproduced by QX_+/V_t.

The same conclusion may also be reached from the results shown in Fig. 4.2f for different values of v_m.

In Fig. 4.2g, scaled impulse data are shown for four widely different chamber volumes V_i with $A_j'/A_k=1/2$, $v_m = 90^o$, and L/D = 21,6. As may be seen, the data are relatively insensitive to V_i.

Finally, Fig. 4.2h shows an example of the reduction in scaled impulse with decreasing values of the ratio A_j'/A_k.

As for front pressure, various empirical scaling relationships with Eq. (2.1b) as basis were fitted to the experimental results. In particular, a reasonable fit to all the data was obtained using the following expression:

$$I\, A_k/Q = E_1(QX_{\pm}/V_t)^{E_2}(A'_j/A_k)^{E_3}\exp(-E_4\, L/D)\ldots(4.2)$$

Here, E_1 E_2, E_3, and E_4 were introduced as scaling parameters. The result of this procedure are shown in Table 4.2. As expected, the scaling parameters are relatively uncertain, but Eq. (4.2) reproduces all the data with an average scatter of approximately 30%. This is quite satisfactory considering the relatively large uncertainties involved in the interpretation of the impulse.

The simple relationship in Eq. (4.2) is expected to be invalid for significant wall roughness as for tunnels blasted out of rock. The use of Eq. (4.2) in this case will probably produce result which are quite conservative or on the safe side.

4.3 Scaling Relationships for Positive Duration

The result and the interpretation of the positive duration data show similar characteristics as for the impulse data discussed in Sec. 4.2. The comments made there essentially also apply here. As for the impulse data, a reasonable fit obtained using an expression:

$$t_+A_k/Q = F_1(QX_{\pm}/V_t)^{F_2}\,(A'_j/A_k)^{F_3}\,\exp\,(-F_4\, L/D)\ldots(4.3)$$

Here, F_1, F_2, F_3, and F_4 act as scaling parameters. The results of the nonlinear least squares fit of Eq. (4.3) to all the data are shown in Table 4.3. This fit reproduces all the results with an average scatter of approximately 30% which again is quite satisfactory considering the large uncertainties

involved in the interpretation of the experimental results.

4.4 Comparison With Large Scale Tests

Comparison of the present model tests with a limited number of large scale tests with similar tunnel systems, indicates that the proposed midified scaling laws are valid for engineering purposes. As an example, some results from a large scale test performed by the Norwegian Defence Research Establishment /10/ are included. Using the notation in Fig. 3.b, the storage site parameters were: V_i = 26 m^3, A_j' = 1,5 m^2, A_k = 17 m^2, and V_m = 90°. The TNT charges detonated in the storage chamber varied between 56 and 1500 kg, and measurements were performed at distances $L/D \simeq 1 - 3$.

In Fig. 4.4 we show the measured peak pressures versus Q/V_t. As may be seen, these results are in fair agreement with the model data for $A_j'/A_k = 1/8$. It should be noted that the large scale storage chamber was relatively small compared to the cross section of the main passage-way and the L/D-values were also relatively small and in fact outside the range of parameters used in the model test.

5. SUMMARY AND CONCLUSIONS

In this paper an extensive series of model tests on blast wave propagation in the tunnel systems of typical underground ammunition storage sites have been briefly reviewed. Several empirical cross checks of the data from 18 different model configurations have shown that the peak pressure results are consistent with the proposed scaling laws which combine a wide range of important geometrical parameters. In particular, the peak pressure in the main passage-way can be found using an effective loading density $QX_{\pm}/V_t$, where V_t again represents the total volume to the observation point, and the parameter $X_{\pm}$ includes the effects from variable angles between the branch and main passage-way.

The presence of non-scaling parameters (e.g. tunnel wall roughness) makes it difficult to present a formal basis for the validity of the proposed scaling. However, direct comparisons of the present results with a limited number of large scale tests with similar tunnel systems, have shown that the proposed modified scaling laws are valid for engineering purposes.

REFERENCES

1. A. Skjeltorp, T. Hegdahl, and A. Jenssen, "Underground Ammunition Storage I: Test programme, instrumentation and data reduction". Technical nota no 80/72, Norwegian Defence Construction Service (1972).

2. A. Skjeltorp, T. Hegdahl, and A. Jenssen, "Underground Ammunition Storages II A and II B. Chamber Pressure". Technical note no 79/72, Norwegian Defence Construction Service (1975).

3. A. Skjeltorp, T. Hegdahl, and A. Jenssen, "Underground Ammunition Storages III A and III B: Single Chamber Storage with variable tunnel diameter and variable chamber volume". Technical note no 81/72, Norwegian Defence Construction Service (1975).

4. A. Skjeltorp, T. Hegdahl, and A. Jenssen, "Underground Ammunition Storage V A and V B: Connected chamber storage. Blast load on doors in two sites". Technical note no 83/72, Norwegian Defence Construction Service (1975).

5. The reports in Refs 2-4 labeled A contain the main results whereas the reports labeled B contain the raw data in the form of pressure-time recordings and tabulated blast wave parameters.

6. See for example W.E. Baker, P.S. Westine, and F.T. Dodge, "Similarity Methods in Engineering Dynamics" (Hyden Book Co., New Jersey, U.S.A., 1973) Ch. 4.

7. G. Fredrikson and A. Jenssen, "Underground Ammunition Storage", Technical note no 59/70, Norwegian Defence Construction Service (1970).

8 F.B. Porzel, "Study of Shock Impedance Effects in a Rough Walled Tunnel", Reseach Paper No. P-330, Institute for Defence Analysis (1969) (AD 684790).

9. A.T. Skjeltorp, "Airblast Propagation Through Tunnels and the Effect of Wall Roughness", Technical note no 103/75, Norwegian Defence Construction Service (1975)

10. D.R. Curran, "Underground Storage of Ammunition. Experiments Concerning Accidental Detonation in an Underground Chamber", Report no. X-111, Norwegian Defence Research Establishment (1966).

Table 4.1.3a Least squares fits of Eq. (4.1.3a) to the peak pressure data for each configuration.

V_i (cm^3)	A_k (cm^2)	A_j'/A_k	Angle v_m (deg)	B_1[a]	B_2	Error[b] %
300	20	½	90	10,3±1,1	0,40±0,03	13
300	20	1/4	90	7,0±1,1	0,40±0,05	19
300	20	1/8	90	4,7±1,1	0,40±0,04	15
800	20	½	90	6,5±1,1	0,55±0,03	14
800	20	1/4	90	4,8±1,1	0,52±0,05	19
800	20	1/8	90	2,8±1,1	0,58±0,03	15
1750	20	½	90	5,2±1,0	0,59±0,02	10
1750	20	1/4	90	3,3±1,1	0,59±0,02	10
1750	20	1/8	90	1,7±1,1	0,67±0,03	14
7250	140	½	90	6,9±1,1	0,63±0,04	12
10900	140	½	90	7,1±1,1	0,41±0,06	23
15200	140	½	90	6,4±1,1	0,50±0,05	19
7250	140	½	60	7,0±1,0	0,58±0,02	13
10900	140	½	60	6,3±1,1	0,54±0,03	14
15200	140	½	60	6,2±1,1	0,57±0,03	13
7250	140	½	35	6,7±1,0	0,54±0,02	12
10900	140	½	35	5,9±1,1	0,58±0,03	12
15200	140	½	35	6,4±1,1	0,54±0,02	13

a. In units where p is in bar, Q in kg TNT and V_t in m^3.

b. The average difference between the fitted curves and experimental data.

Table 4.1.3b Nonlinear least squares fit of Eq.(4.1.3b) to the combined peak pressure data for all configurations. The average difference between the fitted curves and the experimental data is 20%.

Parameter	Numerical value
c_1 [a]	$10,0 \pm 0,3$
c_2	$0,548 \pm 0,012$
c_3	$0,61 \pm 0,03$

[a] In units where p is in bar, Q in kg TNT, and V_t in m^3.

Table 4.1.3c Nonlinear least squares fits of Eqs.(4.1.3c) and (4.1.3d) to the combined peak pressure data for all configurations.
The average difference between the fitted curves and experimental data is 20%.

Parameter	Numerical value
D_1 [a]	$9,9 \pm 0,3$
D_2	$0,556 \pm 0,011$
D_3	$0,67 \pm 0,03$
D_4	$-0,19 \pm 0,20$ (mm)

[a] In units where p is in bar, Q in kg TNT, and V_t in m^3.

Table 4.2 Nonlinear least squares fit of Eq. (4.2) to the reduced impulse data, IA_k/Q, for all configurations. The average difference between the fitted curves and experimental data is 29%.

Parameter	Numerical value
E_1 [a]	$20,8 \pm 0,4$
E_2	$-0,399 \pm 0,013$
E_3	$0,0275 \pm 0,0011$
E_4	$0,25 \pm 0,05$

[a] In units where I is in bar ms, Q in kg TNT, A_k in m^2, and V_t in m^3.

Table 4.3 Nonlinear least, squares fit of Eq (4.3) to the reduced positive duration data, $t_+ A_k/Q$ for all configurations. The average difference between the fitted curves and experimental data is 33%.

Parameter	Numerical value
F_1 [a]	$8,4 \pm 0,3$
F_2	$-0,90 \pm 0,01$
F_3	$0,0349 \pm 0,0008$
F_4	$-0,48 \pm 0,04$

[a] In units where t_+ is in ms, Q in kg TNT, A_k in m^2, and V_t in m^3.

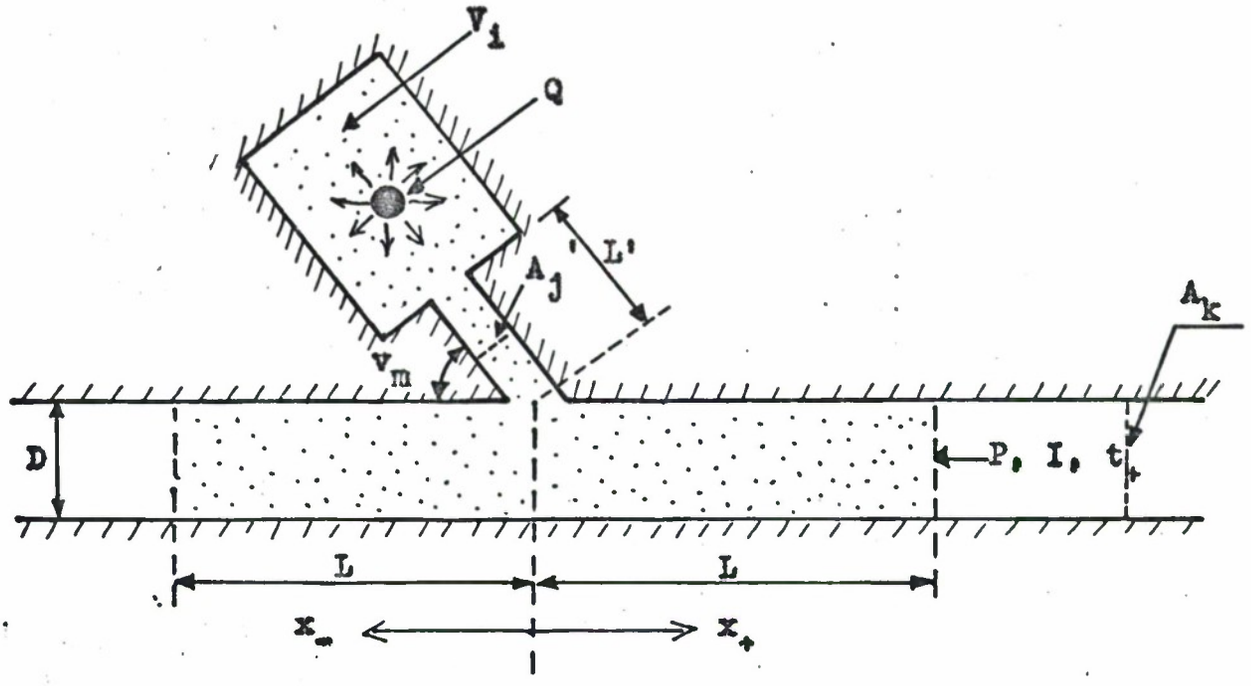

Q = TNT charge

V_i = Chamber volume

L' = Length of branch passage-way

A_j' = Cross-sectional area of branch passage-way

A_k = Cross-sectional area of main passage-way

v_m = Angle between branch- and main passage-way

L = Distance to observation point

D = $\sqrt{4A_k/\pi}$ = Diameter of main passage-way

$V_t = V_i + A_j' L' + 2 A_k L$ = Total effective volume

$X_+ = 2(1 - v_m/108^0)$ = Energy distribution factor, positive direction

$X_- = v_m/90^0$ = Energy distribution factor, negative direction.

Fig. 2.1. Definitions of parameters used for the connected chamber storage sites.

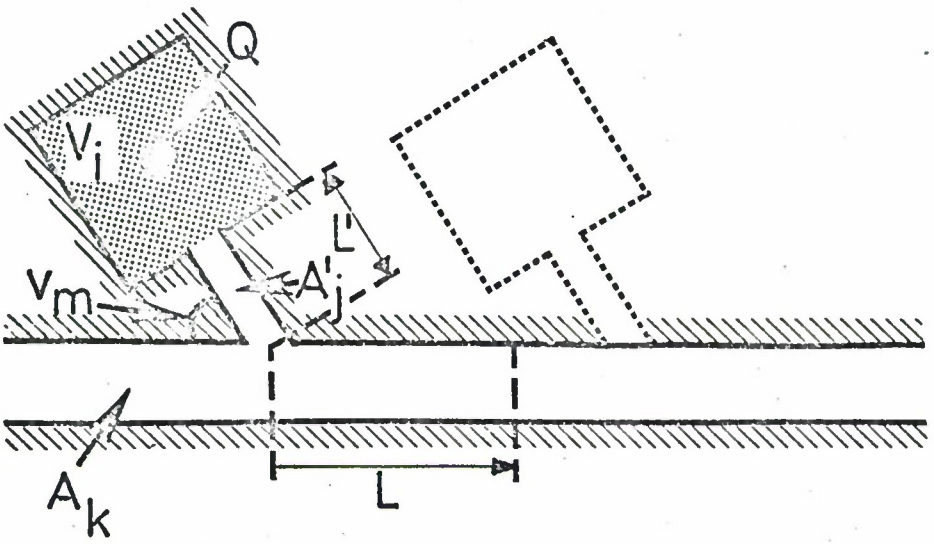

V_i (cm^3)	A_k (cm^2)	A_j' (cm^2)	v_m (deg)
V_1 = 300	A_1 = 20	A_1' = 2,5	v_1 = 35
V_2 = 800	A_2 = 140	A_2' = 5	v_2 = 60
V_3 = 1760		A_3' = 10	v_3 = 90
V_4 = 7250		A_4' = 70	
V_5 = 10900			
V_6 = 15200			

Fig.3.a. Model configurations used in the connected chamber storage tests. A total of 18 different combinations were tested varying the chamber volume V_i, the angle v_m between the branch- and main passage-way and the ratio between the cross sections of the branch- and main passage-way, A_j'/A_k. These configurations were:

$V_i\ A_1\ A_j'\ v_3$ with i = 1, 2, 3, j = 1, 2, 3

$V_i\ A_2\ A_4'\ v_m$ with i = 4, 5, 6, m = 1, 2, 3

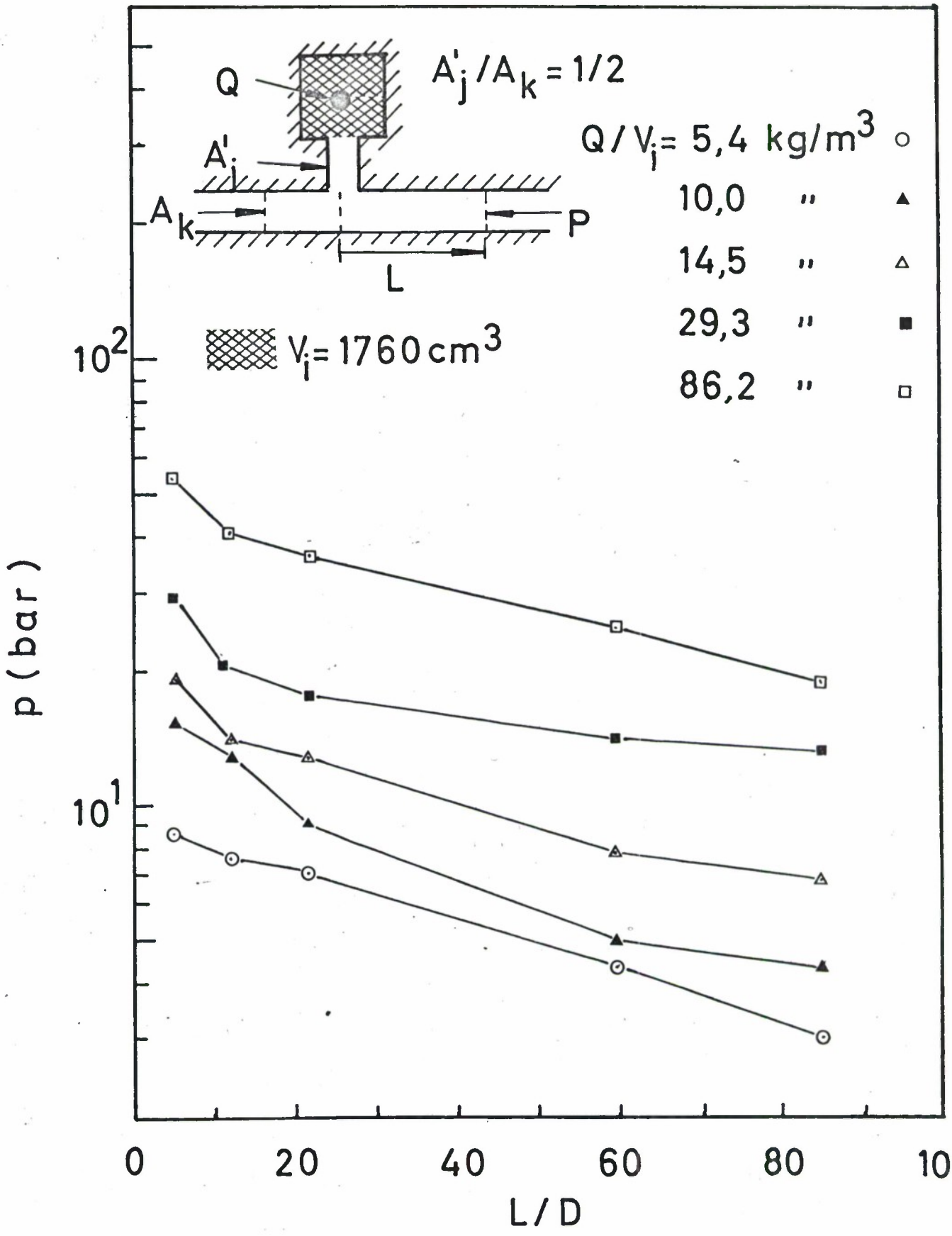

Fig. 4.1a. Peak pressure versus distance in tunnel diameters for various loading densities.

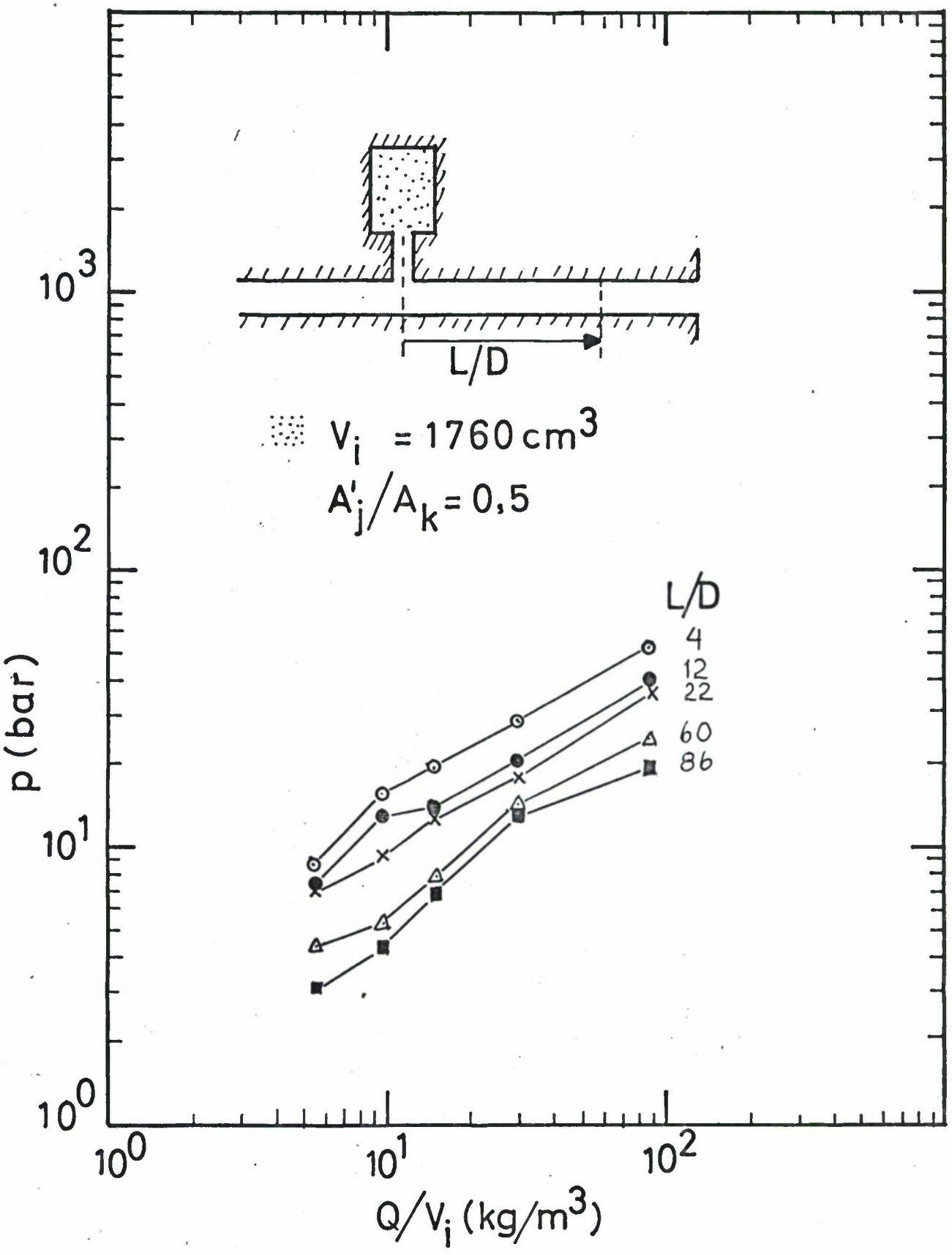

Fig. 4.1b. Peak pressure versus chamber loading density with L/D as parameter.

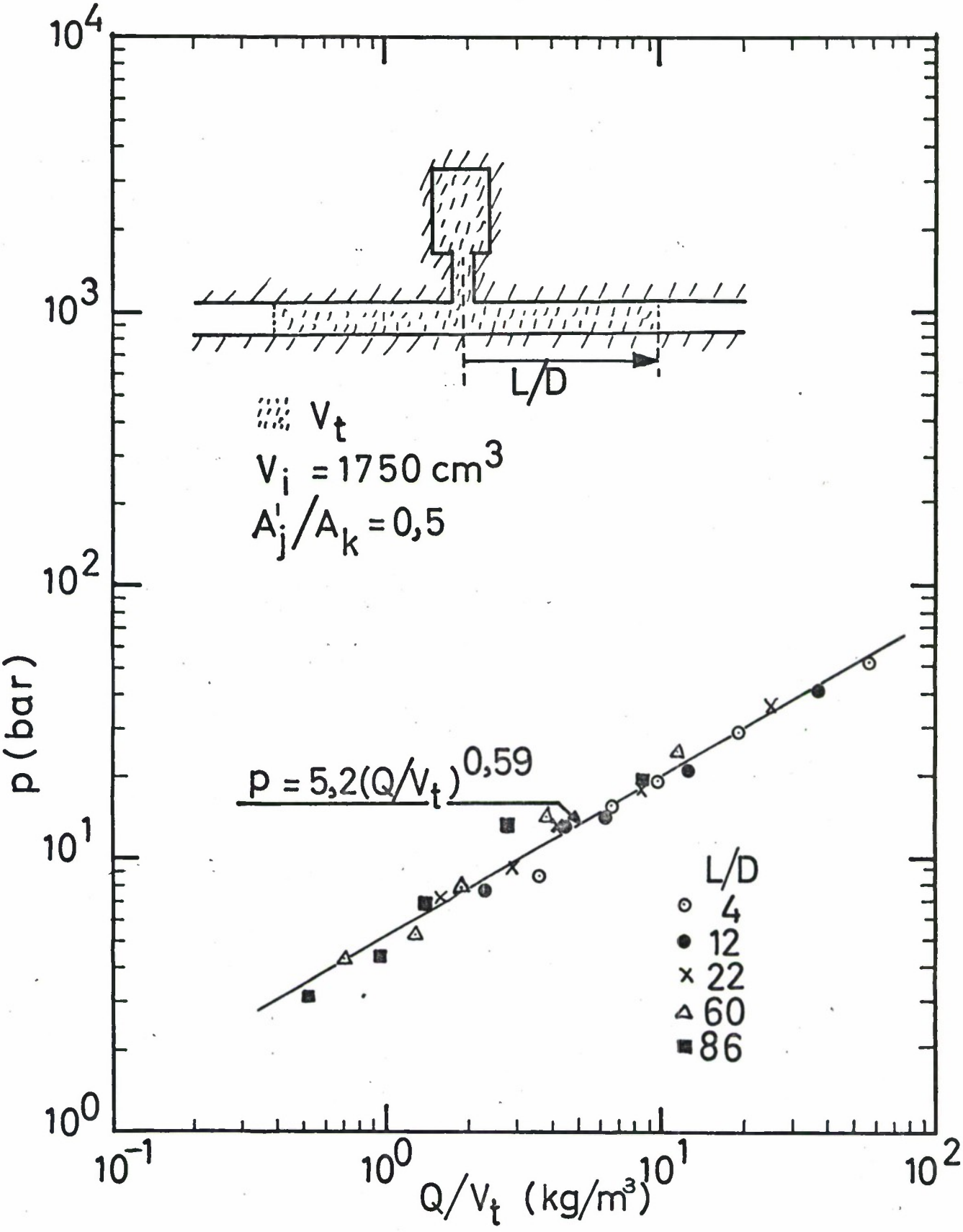

Fig. 4.1c. Peak pressure versus effective loading density, with L/D as parameter. The straight line represents a least squares fit to all the data.

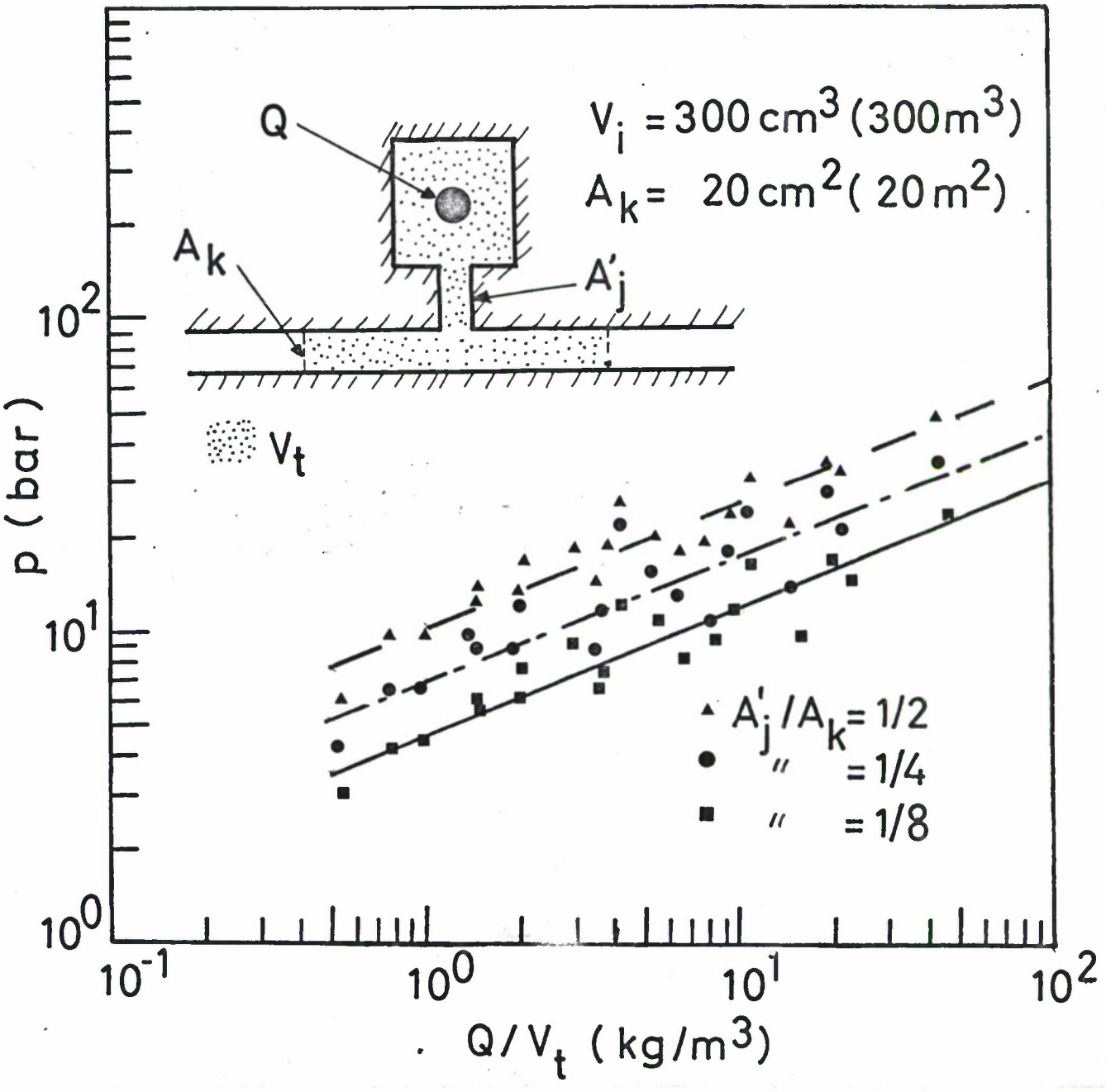

Fig. 4.1d. Peak pressure versus effective loading density for three different values of the ratio between the cross-sections of the branch and main passage-way. Numbers in parentheses refer to a typical full scale site (n = 100). The straight lines represent least squares fits to the data.

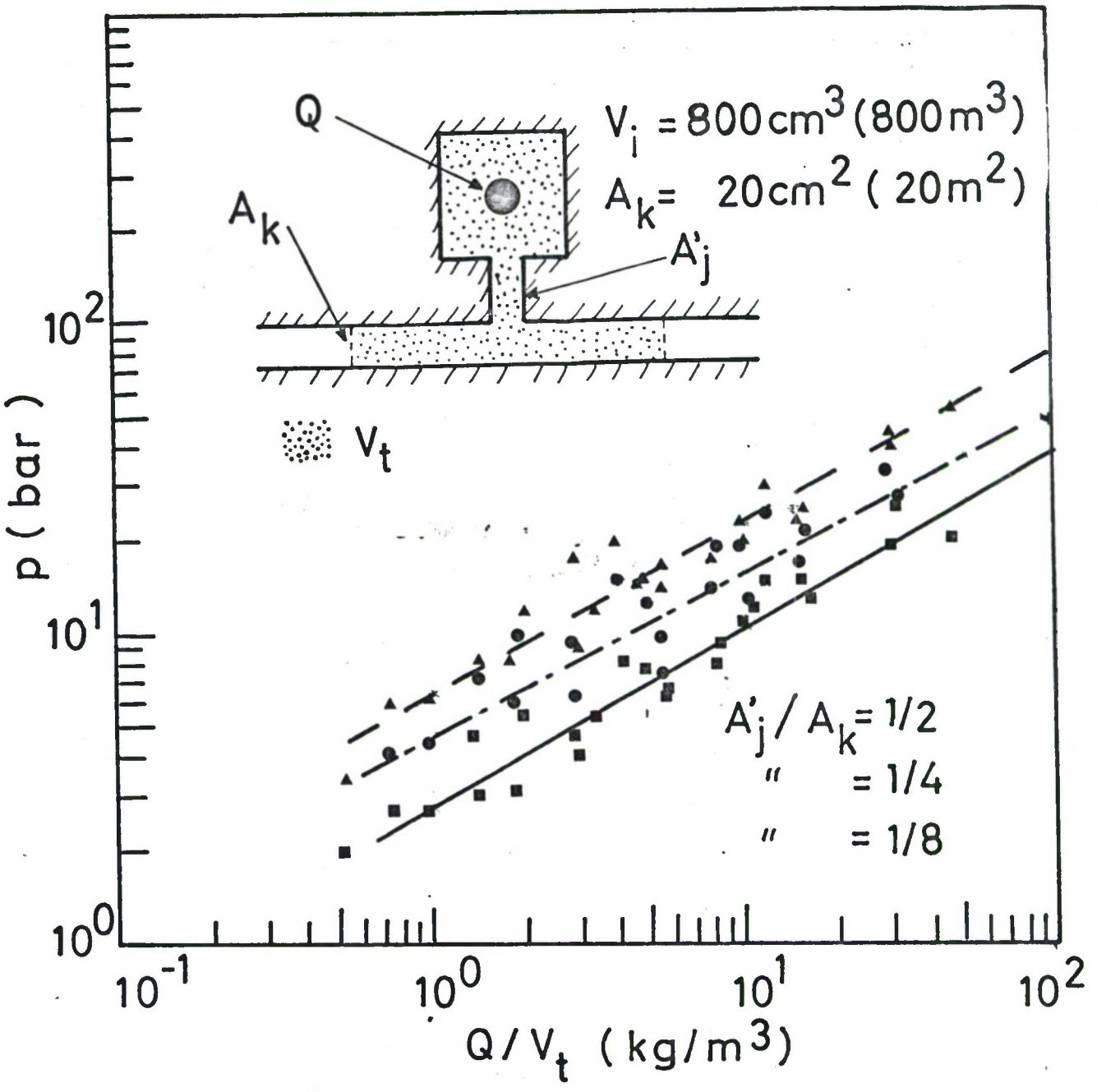

Fig. 4.1e. Peak pressure versus effective loading density for three different values of the ratio between the cross-sections of the branch and main passage-way.
Numbers in parentheses refer to a typical full scale site (n = 100). The straight lines represent least squares fits to the data.

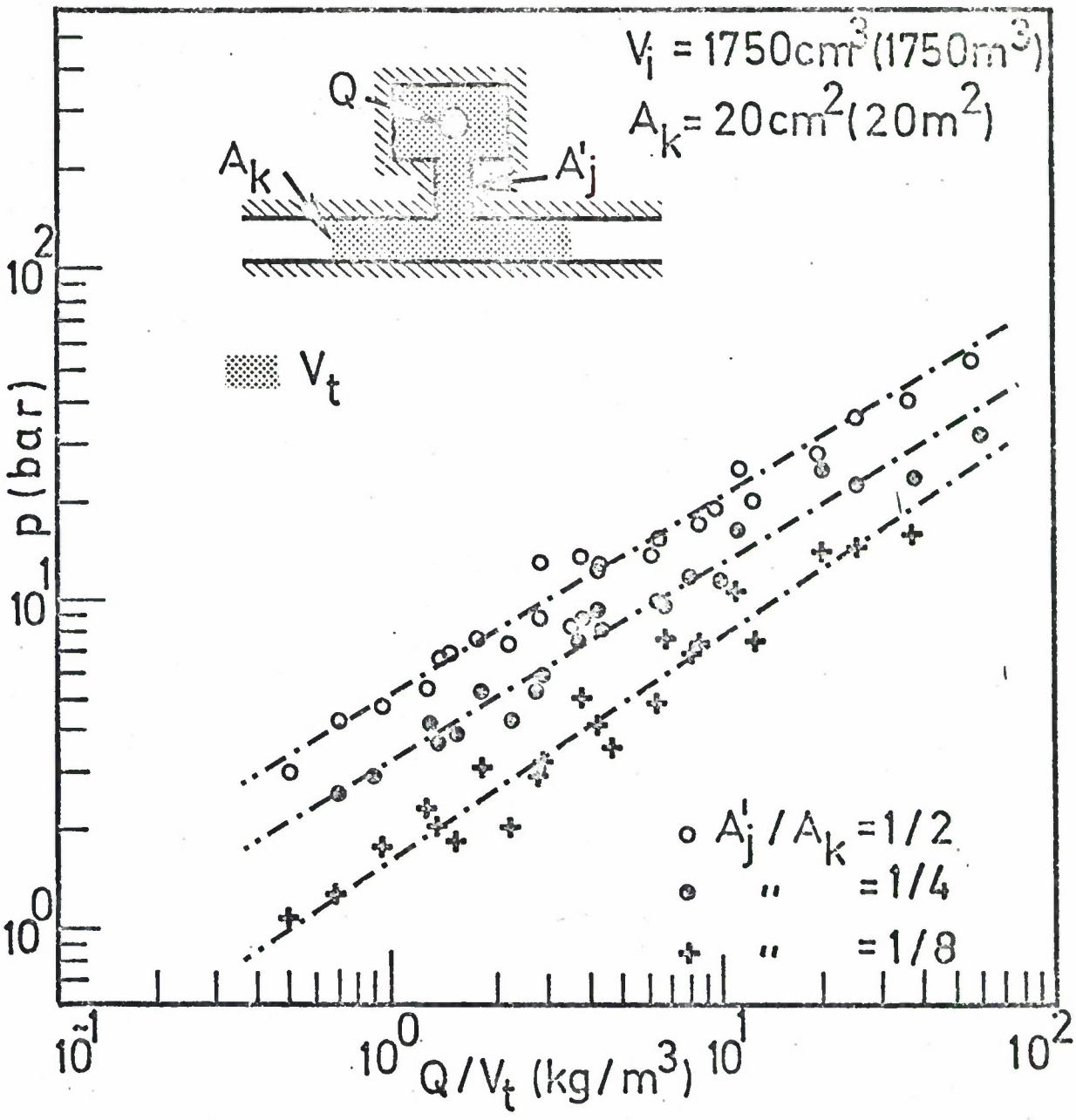

Fig. 4.1f. Peak pressure versus effective loading density for three different values of the ratio between the cross sections of the branch and main passage-way. Numbers in parantheses refer to a typical full scale site (n = 100). The straight lines represent the least squares fits to the data.

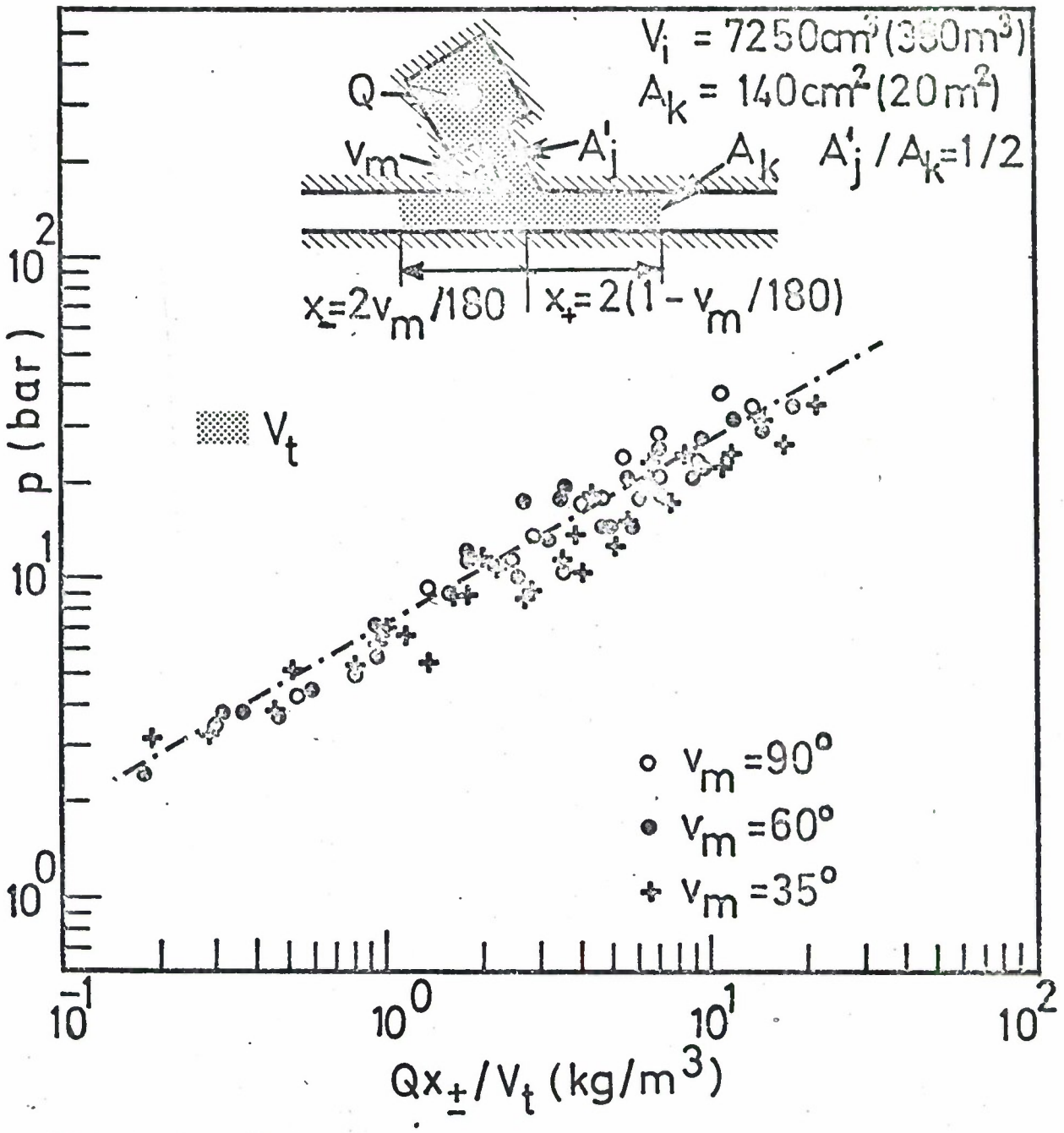

Fig. 4.1g. Peak pressure versus effective loading density for three different values of the angle between the branch and main passage-way. The numbers in parantheses refer to a typical full scale site (n = 38). The traight line represents a least squares fit to all the data.

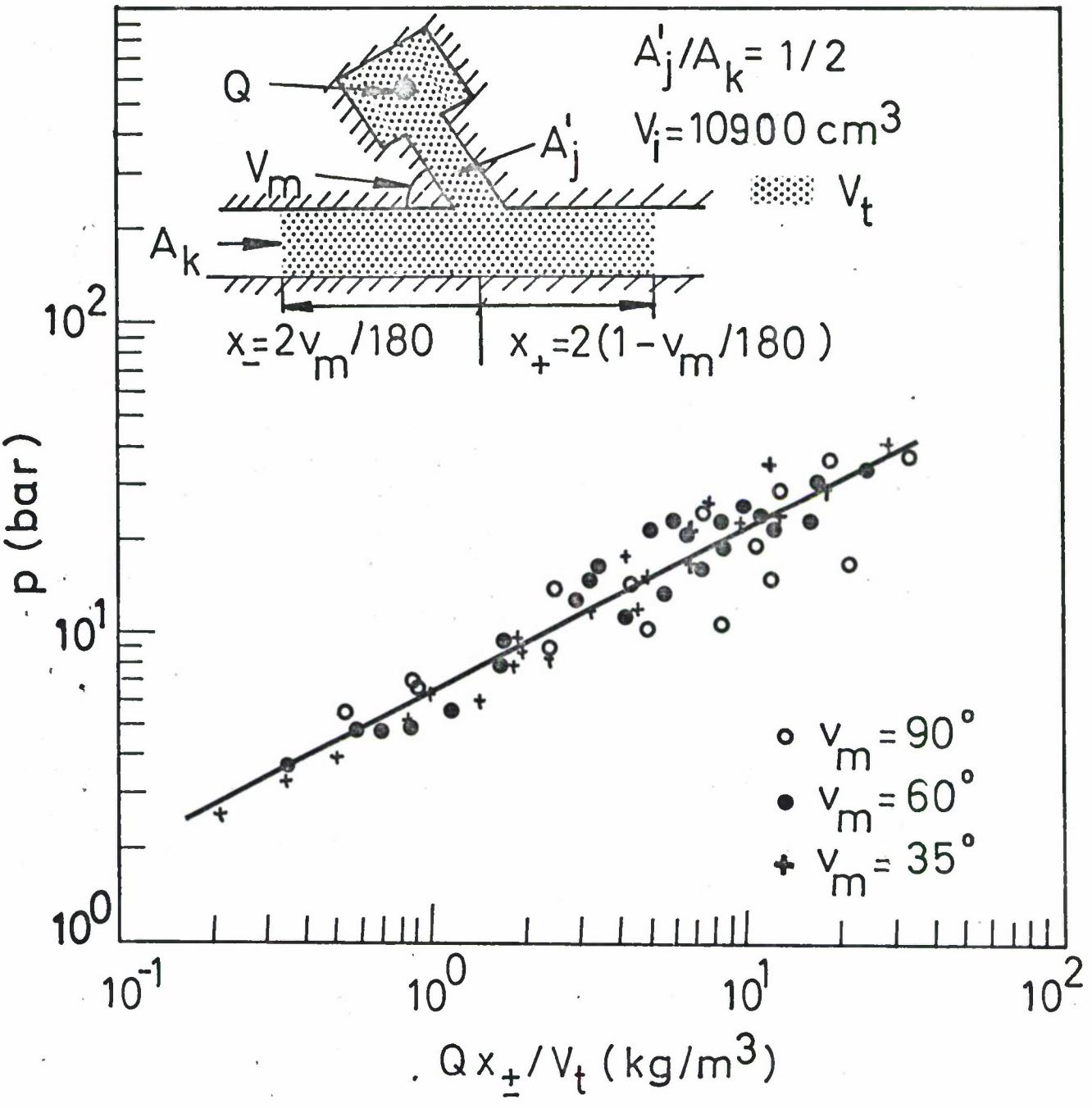

Fig. 4.1h. Peak pressure versus effective loading density for three different values of the angle between the branch and main passage-way. The straight line represents a least squares fit to all the data.

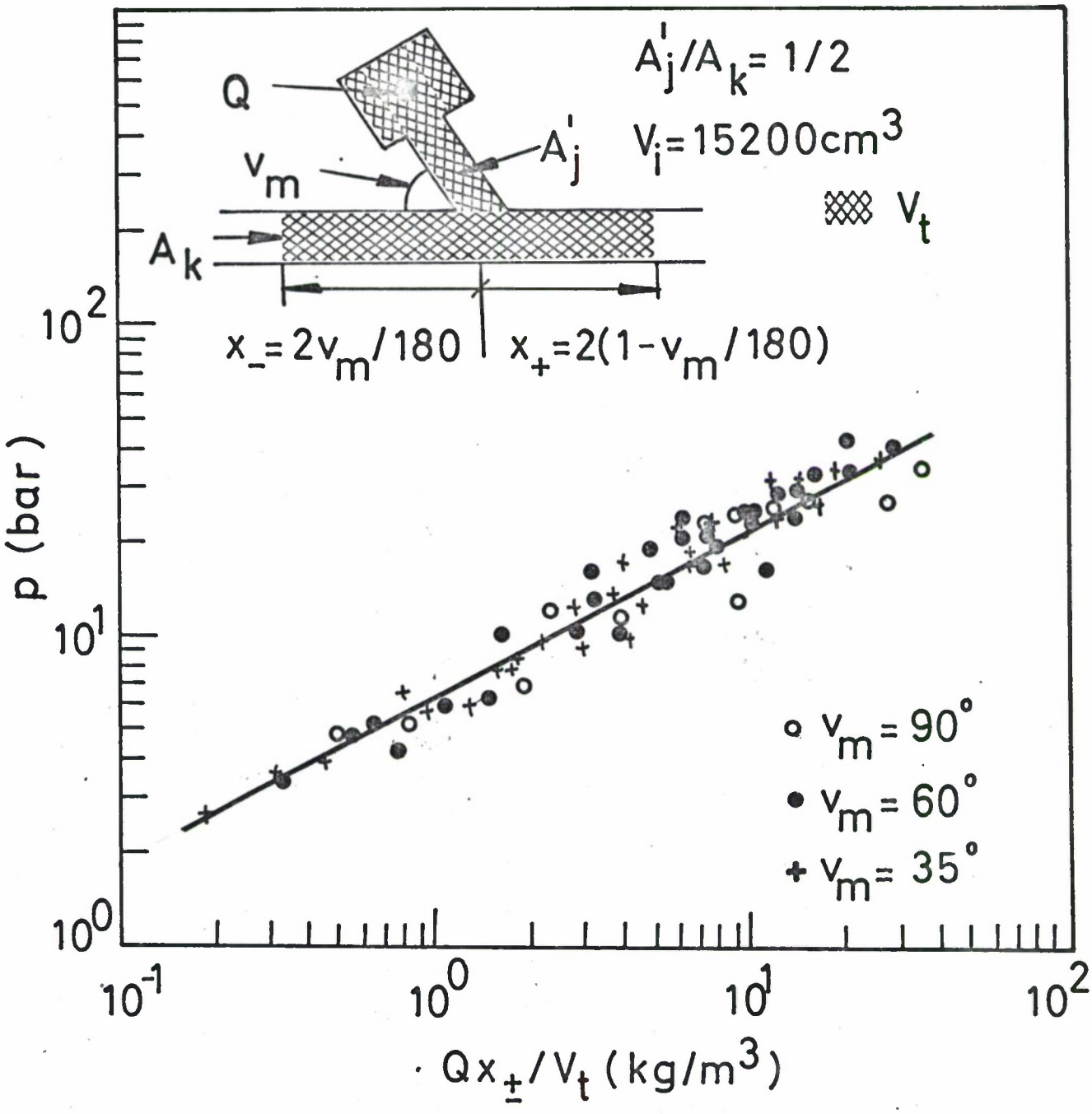

Fig. 4.1i. Peak pressure versus effective loading density for three different values of the angle between the branch and main passage-way. The straight line represents a least squares fit all the data.

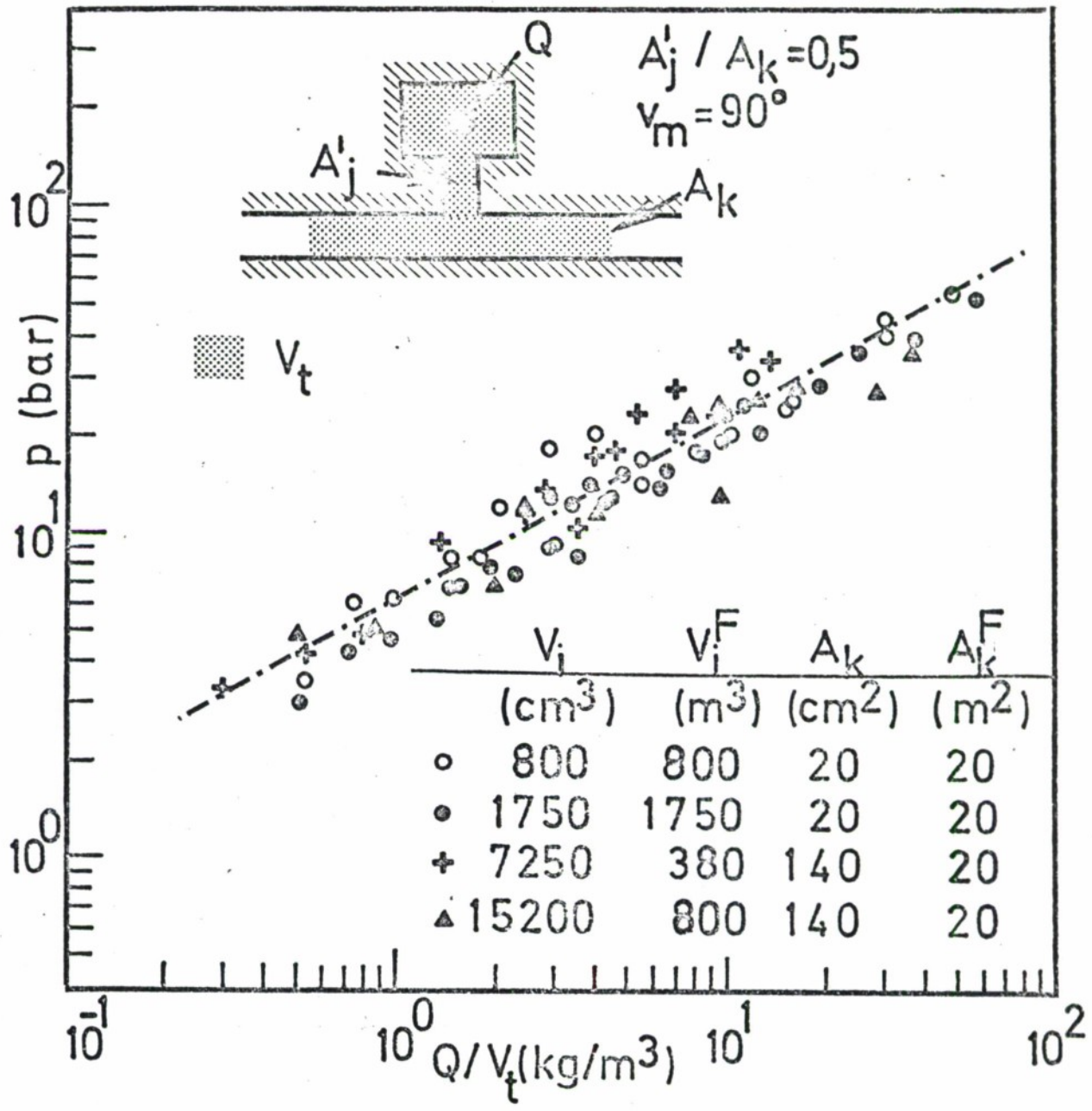

Fig. 4.1j. Peak pressure versus effective loading density in multiple chamber storage sites for four different chamber volumes. With a typical full scale value A_k^F = 20 m^2 for the main passage-way cross-section, the corresponding full scale chamber volumes are listed under V_i^F.

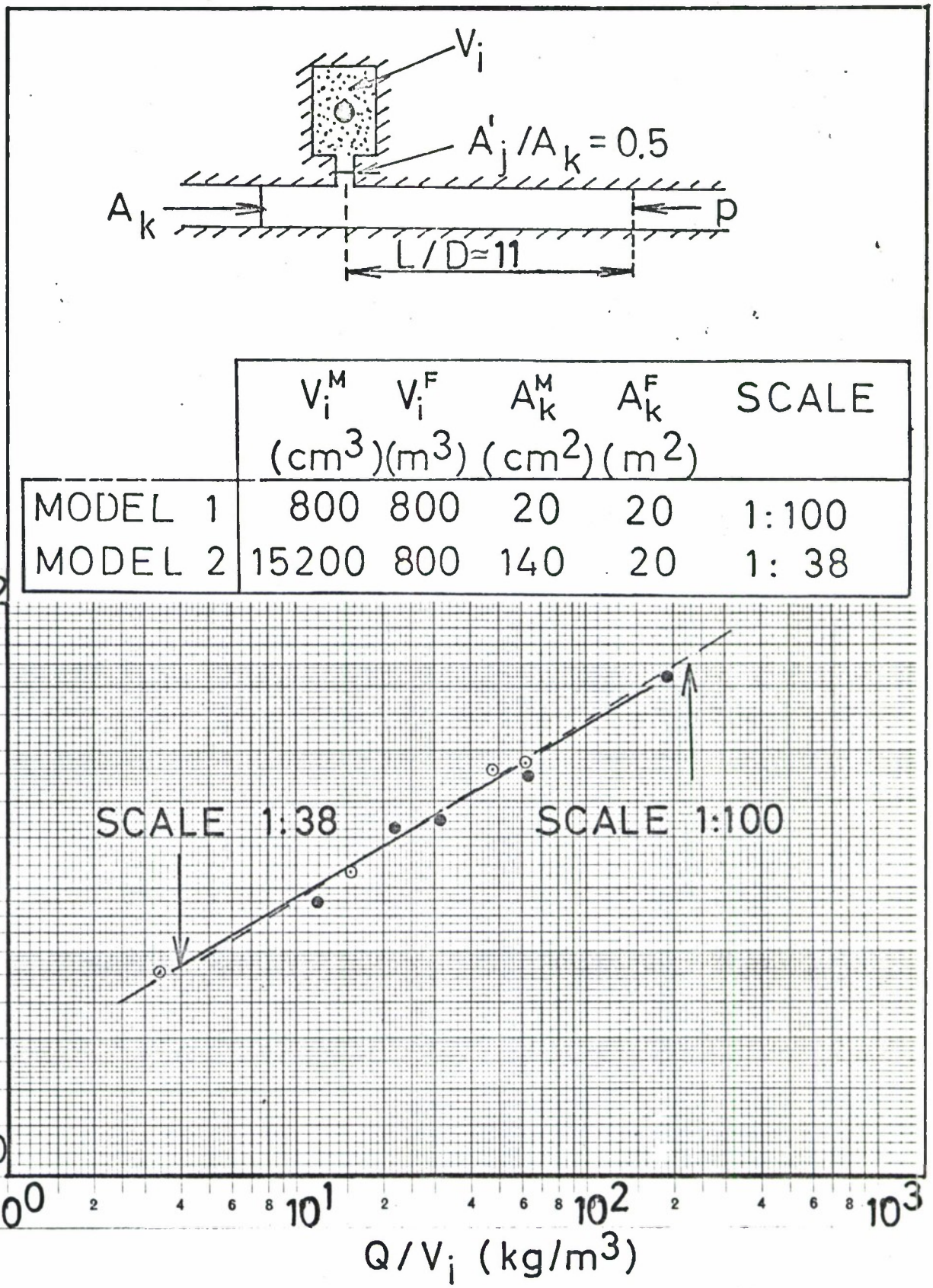

	V_i^M (cm^3)	V_i^F (m^3)	A_k^M (cm^2)	A_k^F (m^2)	SCALE
MODEL 1	800	800	20	20	1:100
MODEL 2	15200	800	140	20	1: 38

Fig. 4.1.1a. Comparison of the peak pressure data versus loading density for two geometrically similar models as discussed in the text.

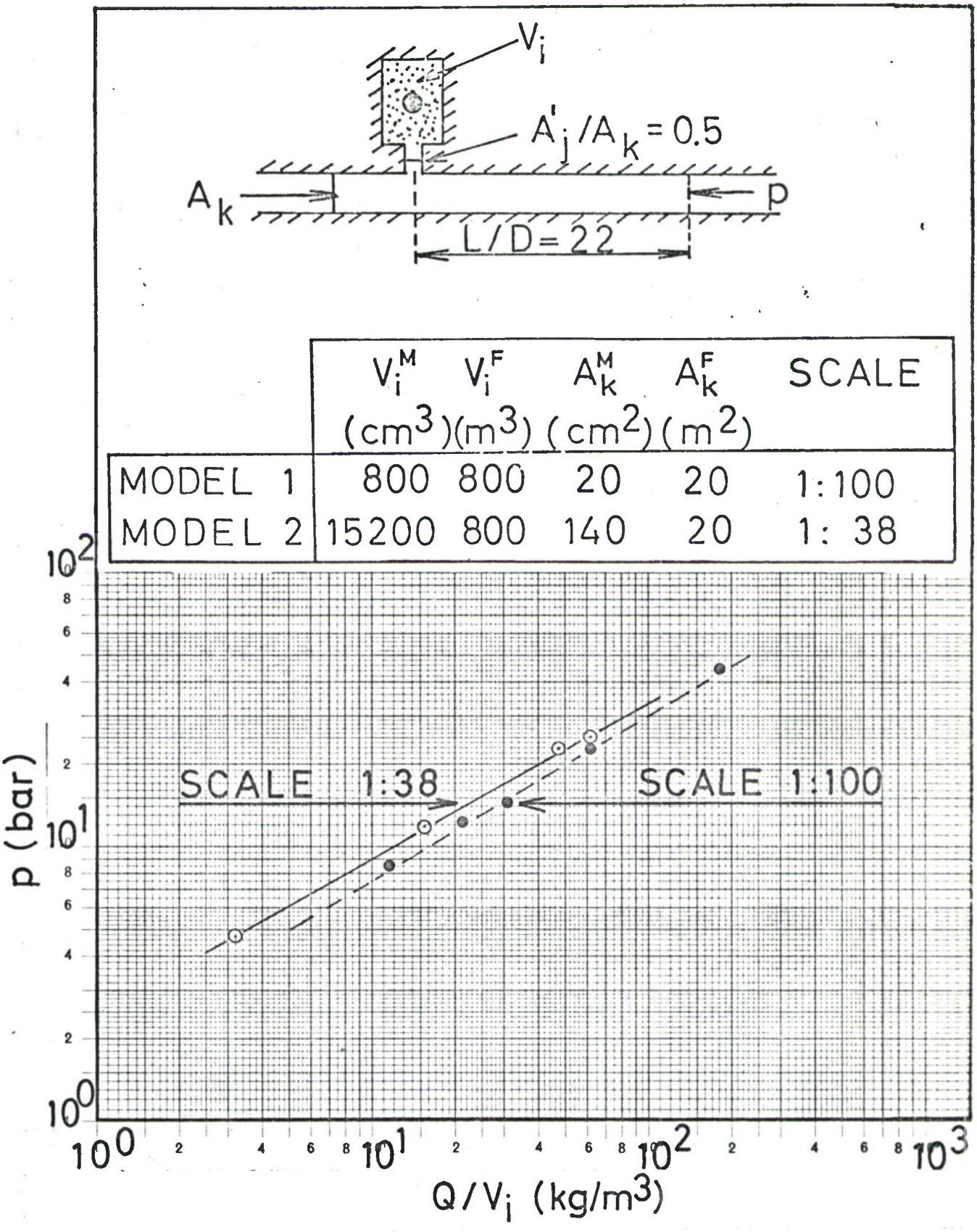

	V_i^M (cm^3)	V_i^F (m^3)	A_k^M (cm^2)	A_k^F (m^2)	SCALE
MODEL 1	800	800	20	20	1:100
MODEL 2	15200	800	140	20	1: 38

Fig. 4.1.1b. Comparison of peak pressure data versus loading density for two geometrically similar models as discussed in the text.

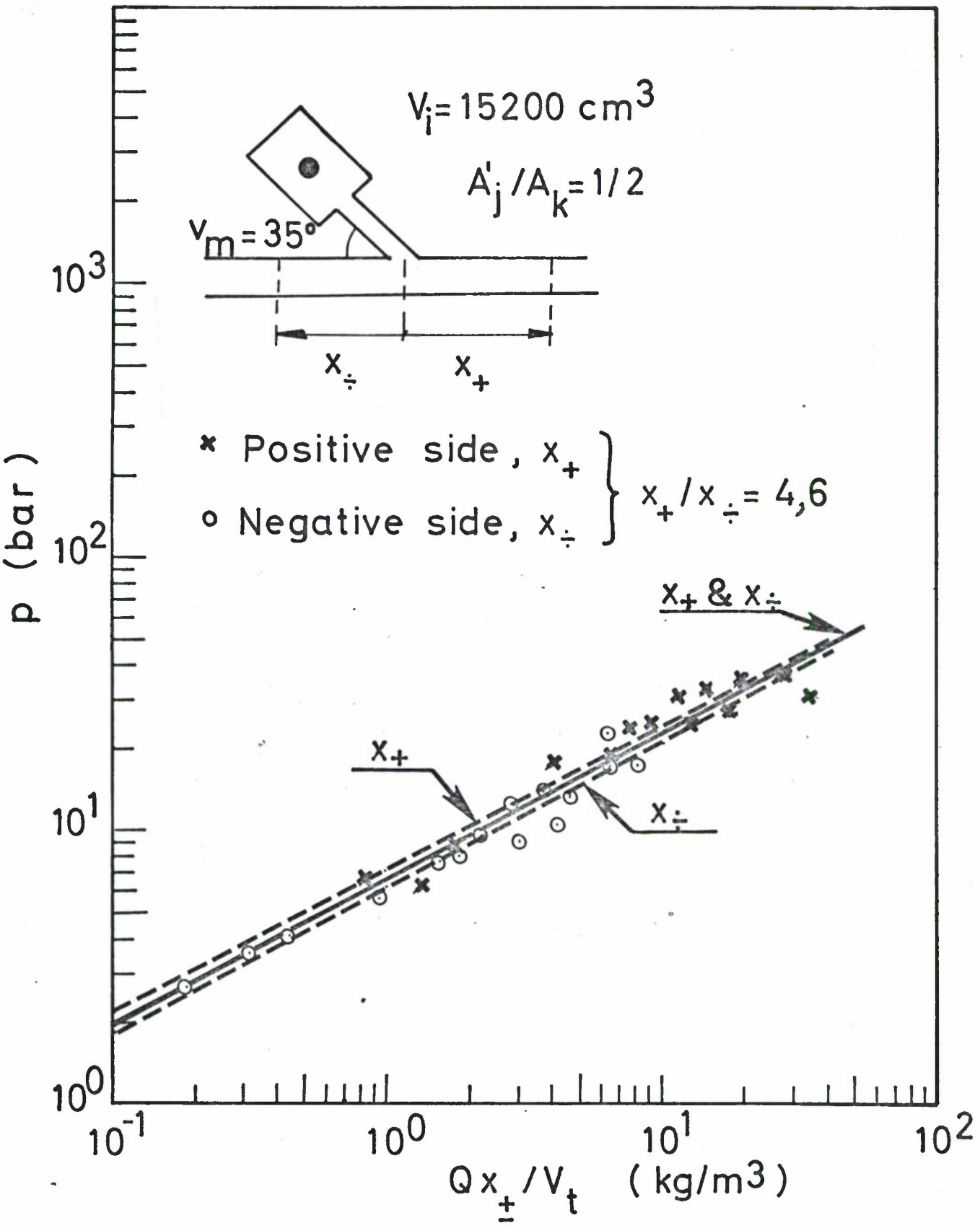

Fig. 4.1.2a. Test of energy distribution in the two directions of the main passage-way as discussed in the text. The dashed lines represent least squares fits to the data for the two directions and the solid line a fit to all the data.

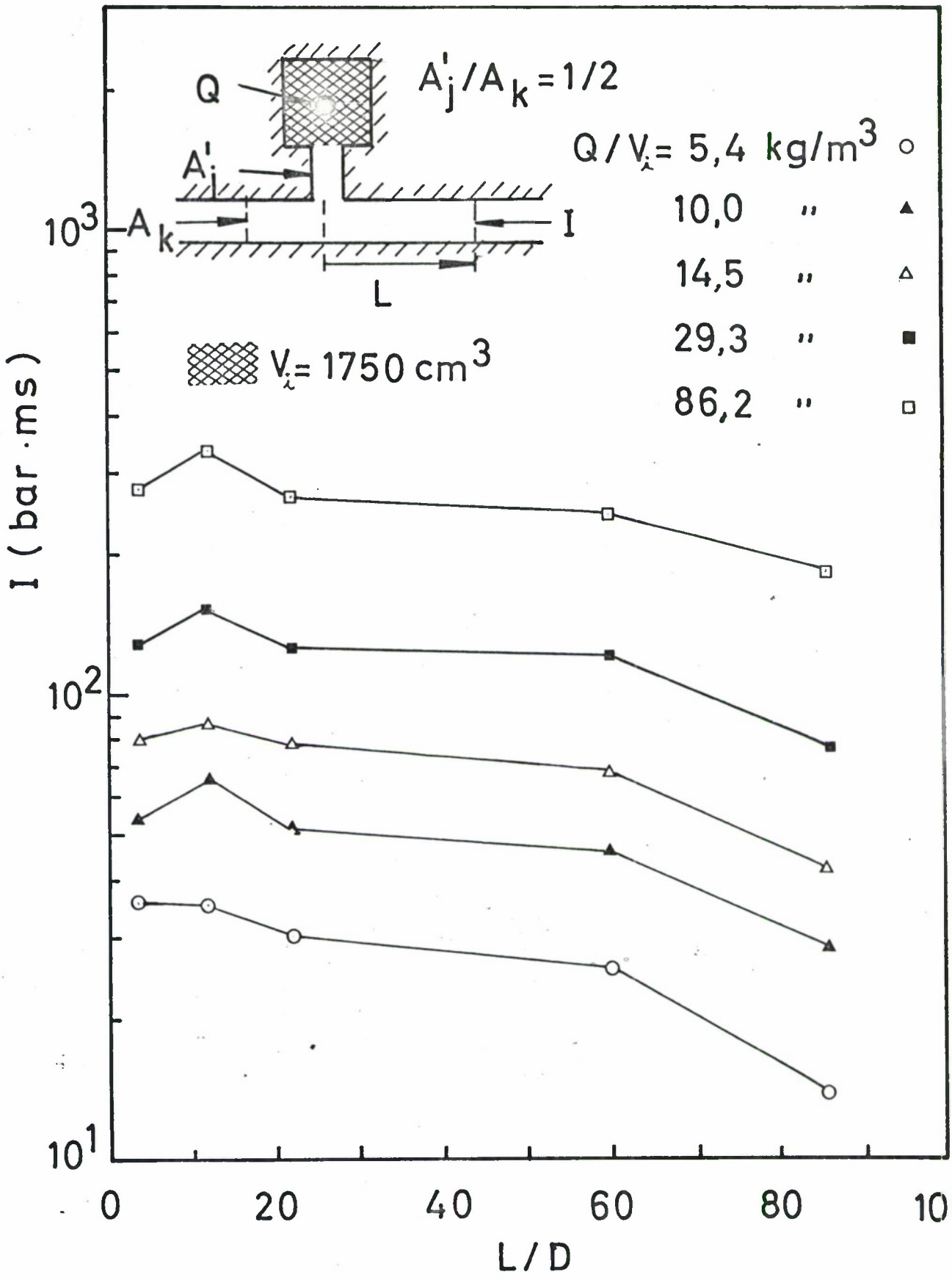

Fig. 4.2a. Impulse versus distance in tunnel diameters for various loading densities.

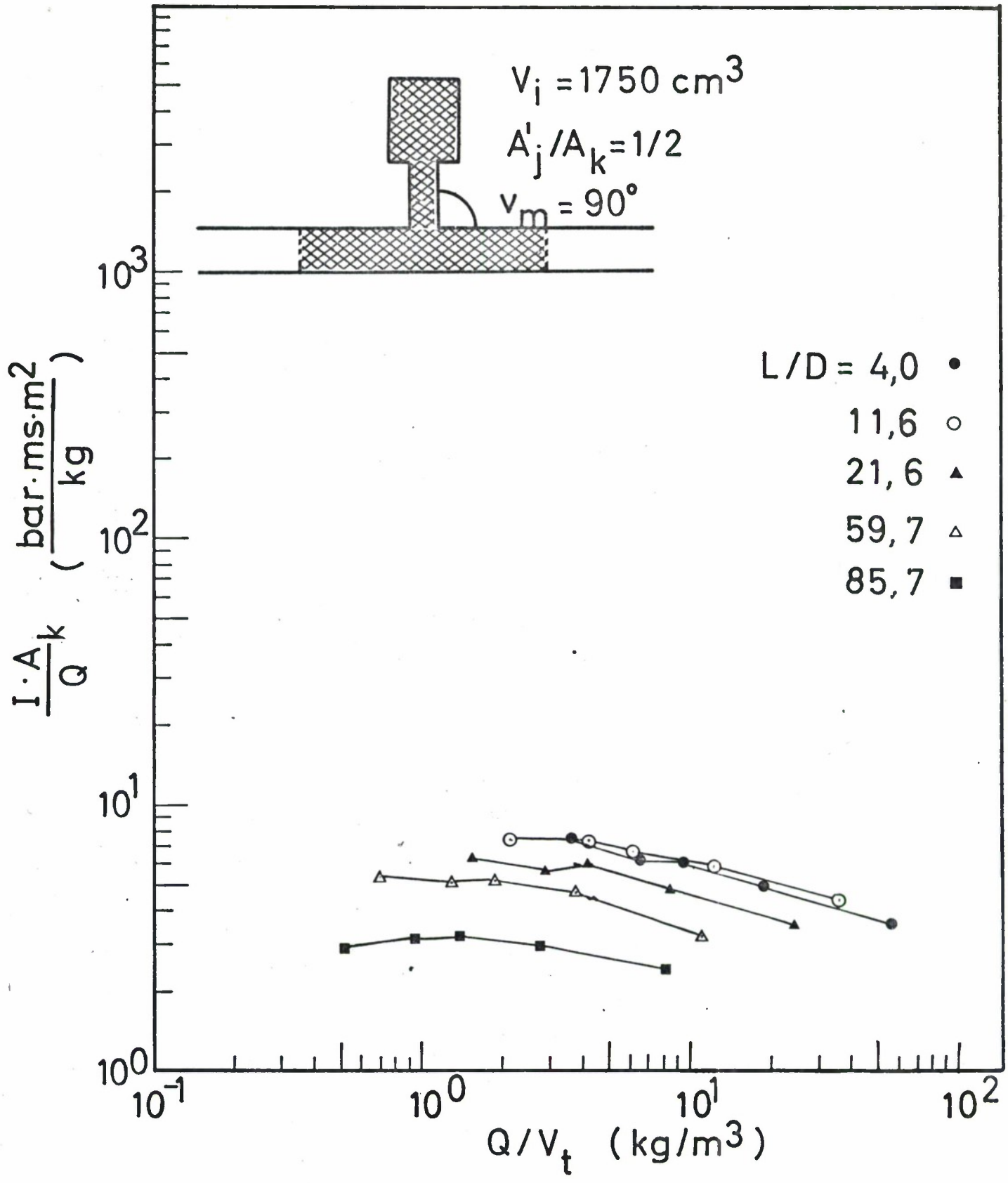

Fig. 4.2b. Scaled impulse versus effective loading density with L/D as parameter.

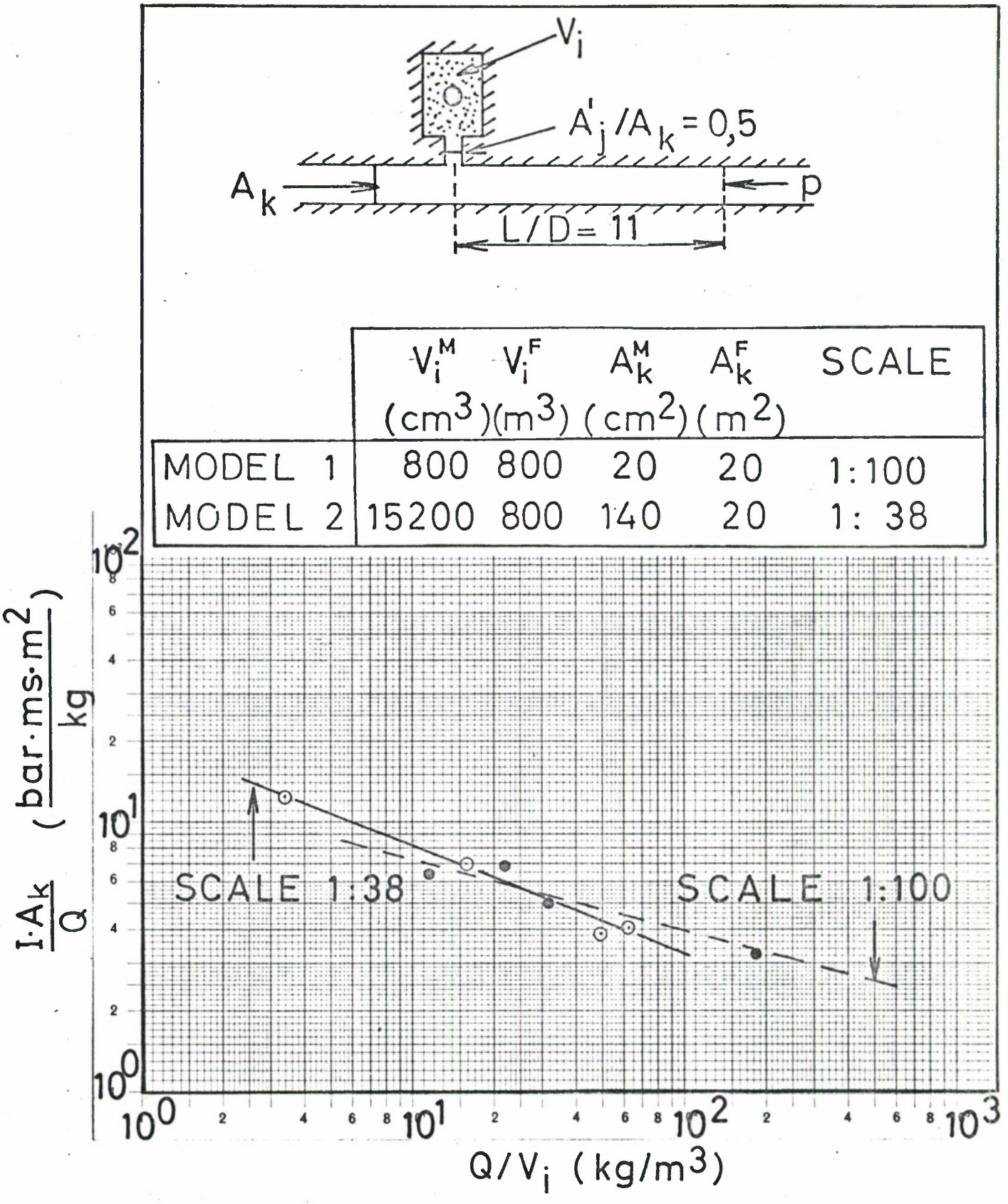

Fig. 4.2c. Comparison of scaled impulse data versus loading density for two geometrically similar models as discussed inn the text.

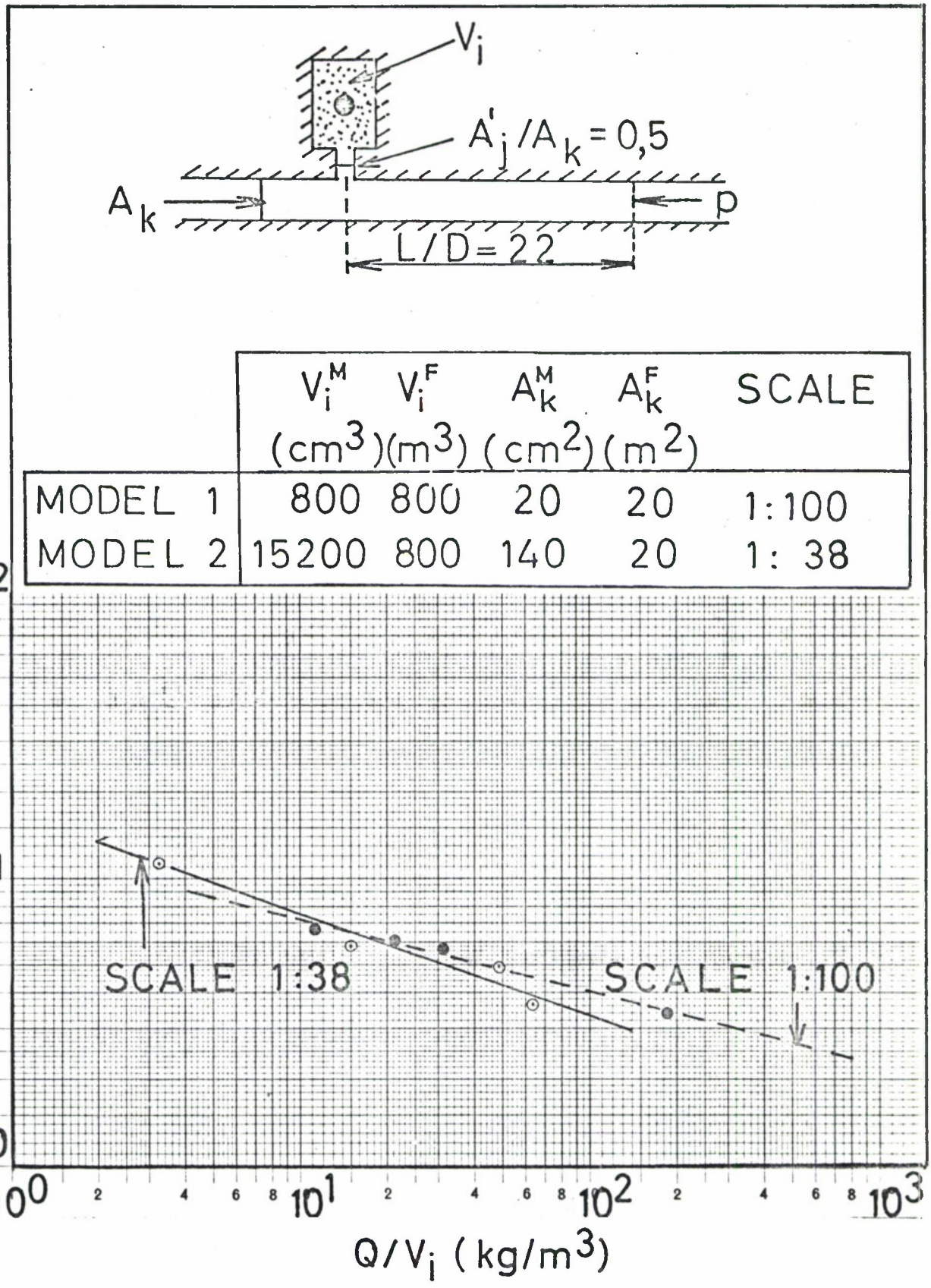

Fig. 4.2d. Comparison of scaled impulse data versus loading density for two geometrically similar models as discussed in the text.

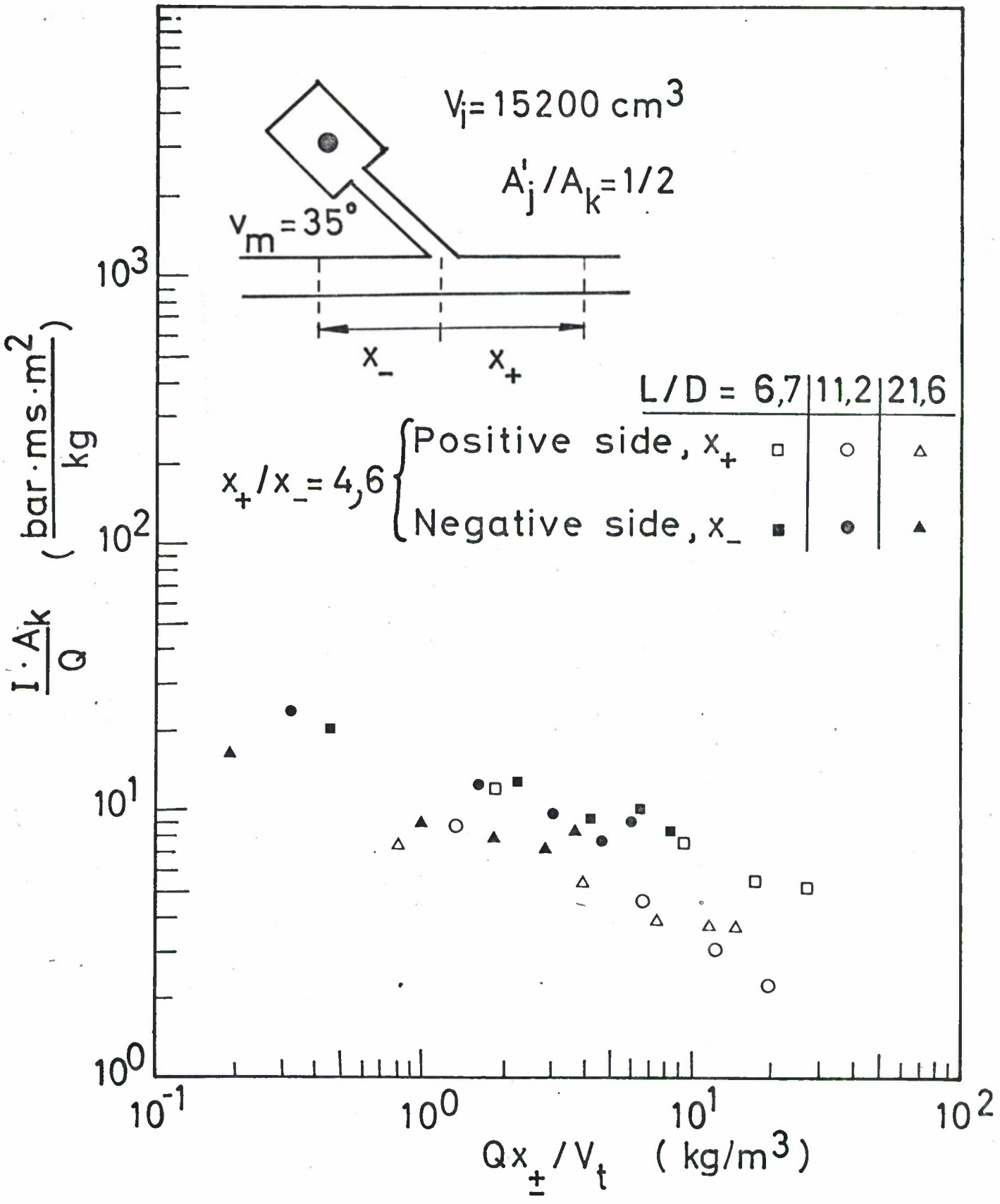

Fig. 4.2e. Scaled impulse versus effective loading density to test the proposed energy distribution.

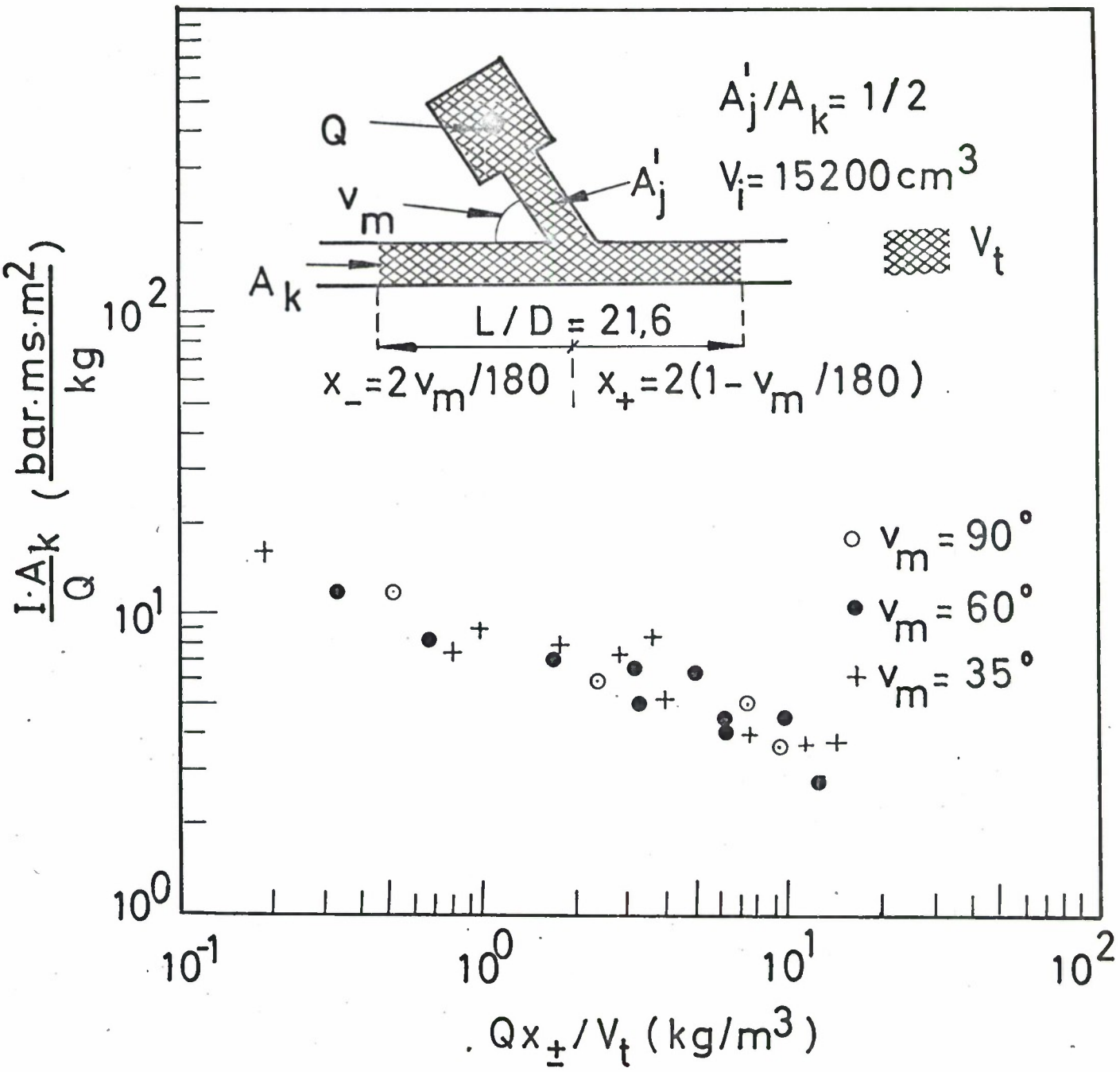

Fig. 4.2f. Scaled impulse versus effective loading density to test the proposed energy distribution.

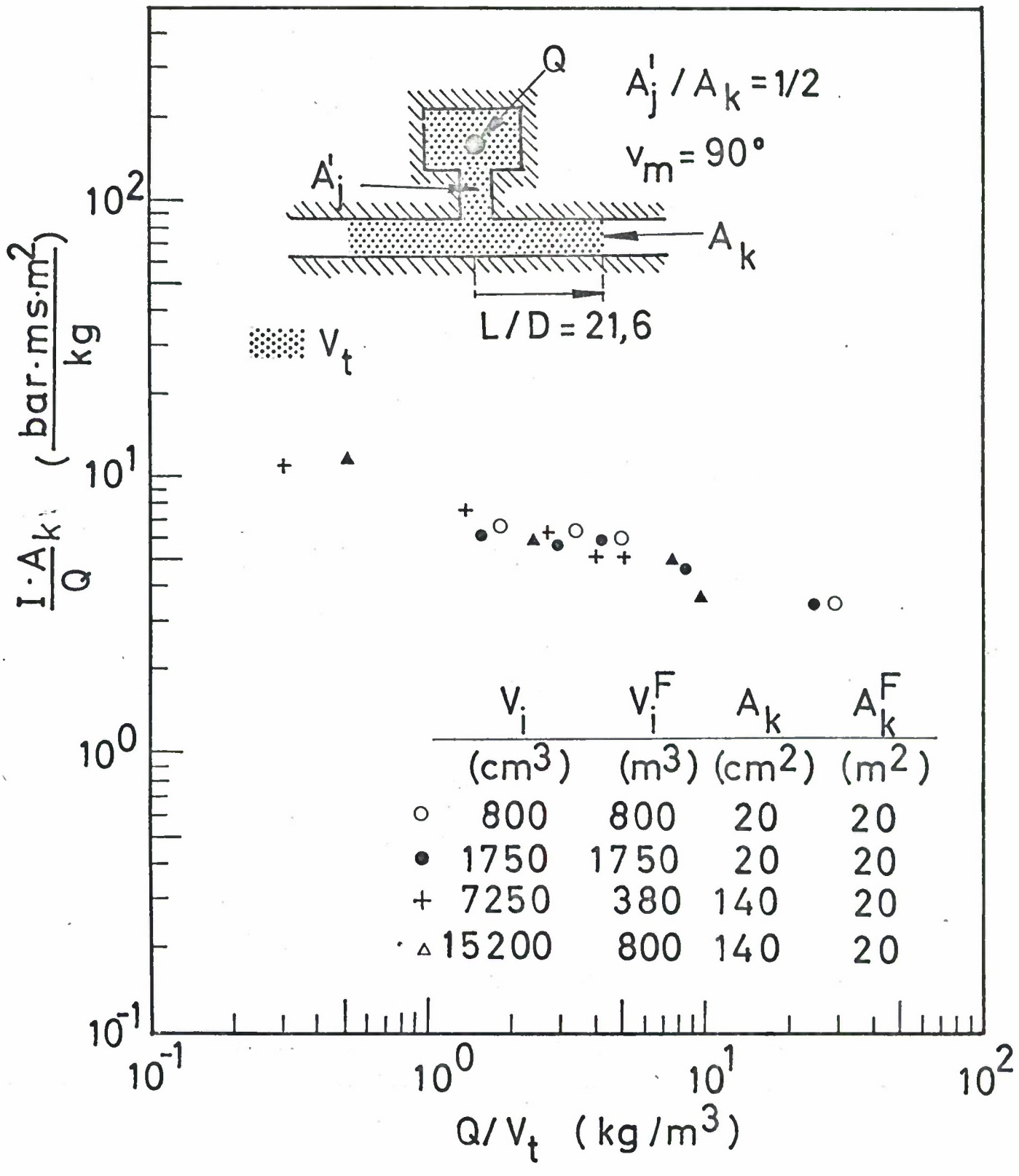

Fig. 4.2g. Scaled impulse versus effective loading density for different chamber volumes.

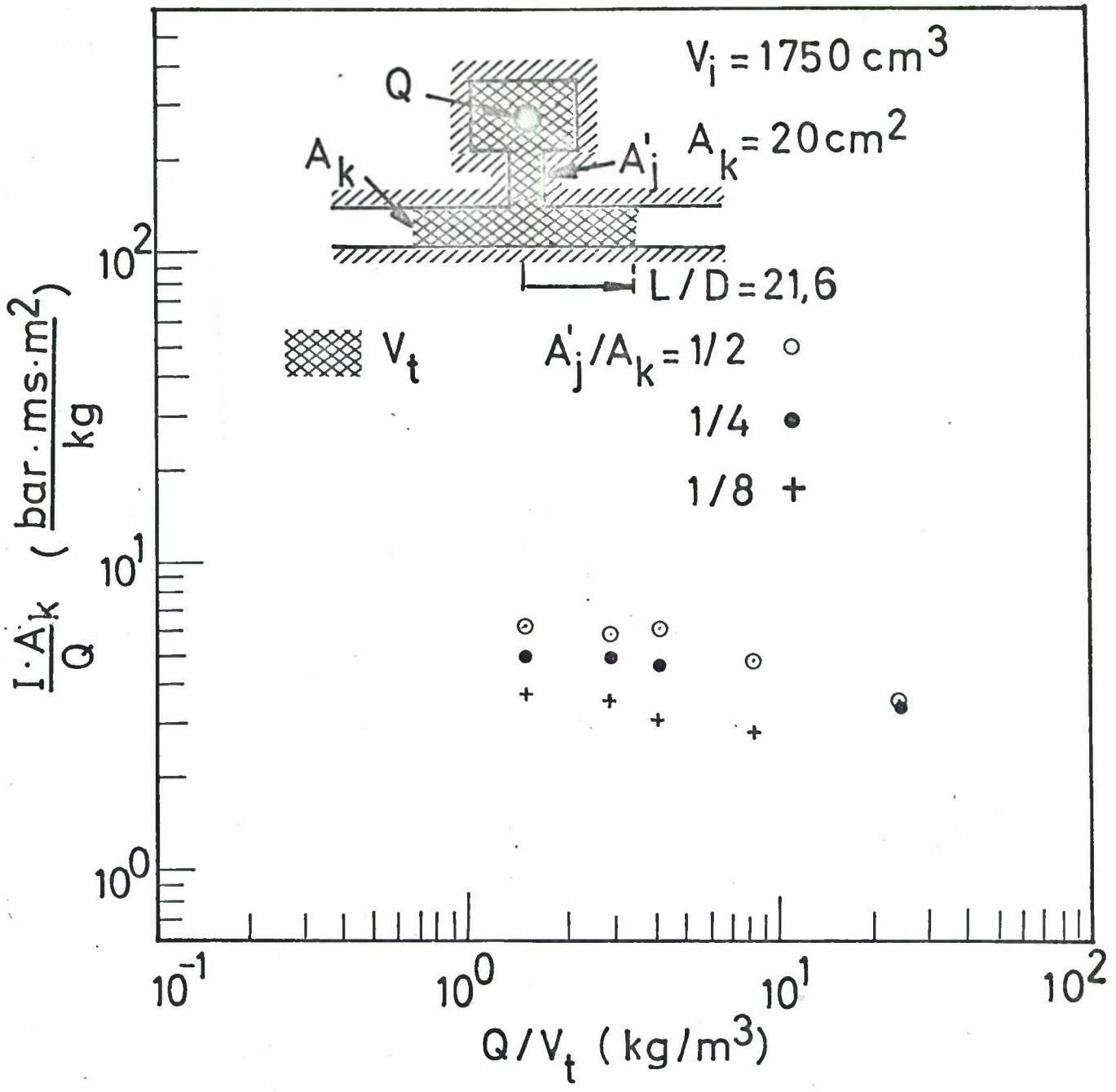

Fig. 4.2h. Scaled impulse versus effective loading density for different ratios of A_j'/A_k.

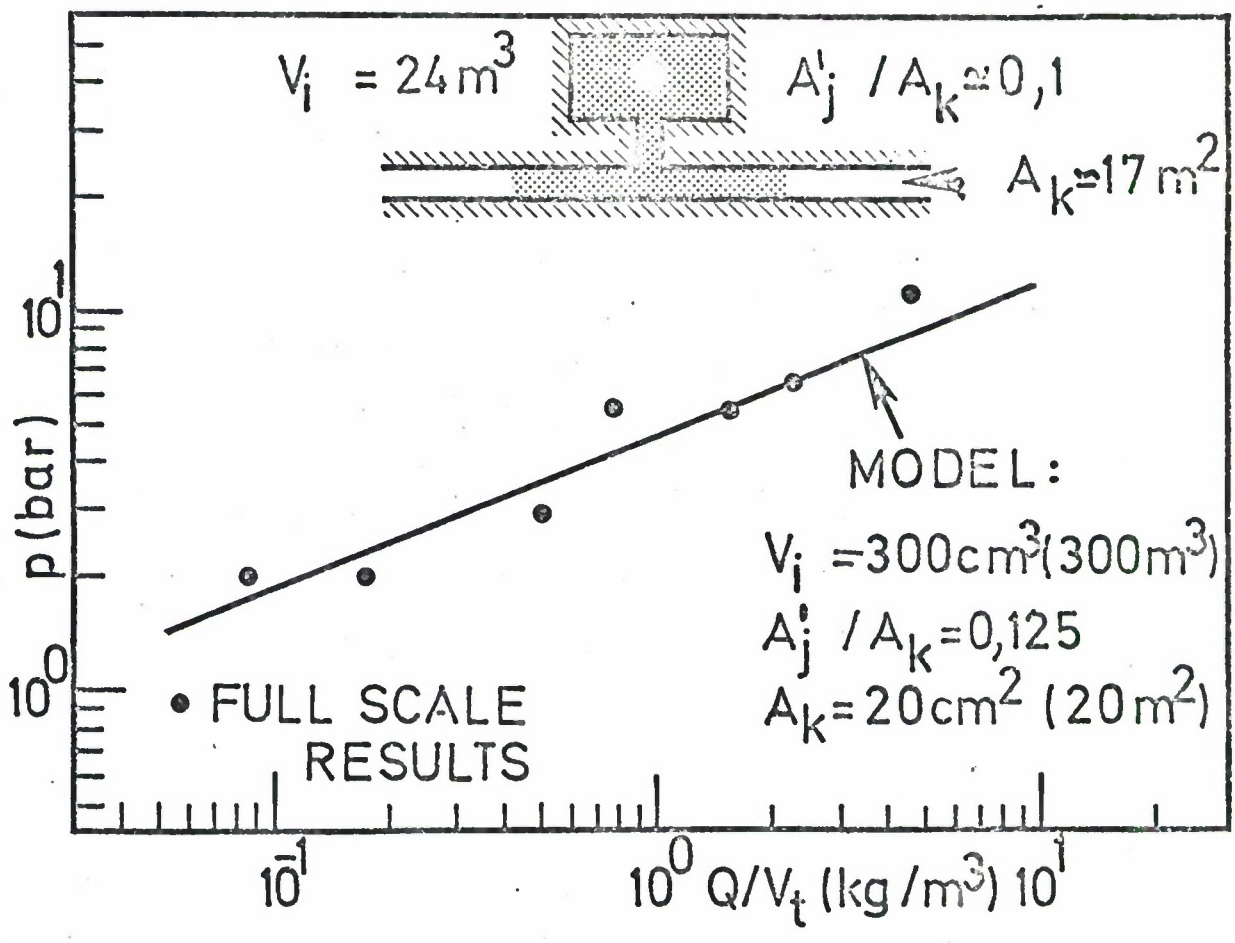

Fig. 4.4. Peak pressure versus effective loading density found in a large scale test /10/ in comparison with model data.